A Scalable Laser-assisted Method to Produce Active and Robust Graphene-supported Nanoparticle Electrocatalysts

Xiaoyong Mo,[1] Kang-Cheung Chan,[2,*] and Edmund C. M. Tse[1,*]

[1] Department of Chemistry, University of Hong Kong, Pokfulam Road, Hong Kong SAR, PRC

[2] Advanced Manufacturing Technology Research Centre, Department of Industrial and Systems Engineering, Hong Kong Polytechnic University, Hung Hom, Hong Kong SAR, PRC

KEYWORDS: Scalable Synthesis, One-step Room-temperature Process, Graphene-supported Nanoparticles, Laser Treatment, Surfactant-free, Binder-free, Liquid waste-free

ABSTRACT: The development of renewable energy schemes requires the scalable production of highly robust electrocatalysts using a sustainable synthesis process that does not generate toxic liquid wastes. Here, an industrial laser system is utilized to prepare electrocatalysts in a continuous fashion using a laser-induced forward transfer (LIFT) method without generating liquid wastes. This dry processing method at room temperature and under ambient pressure enables the production of well-dispersed Pt, Ru, and Ni nanoparticles (NPs) supported on a few-layer graphene carbon framework. This versatile LIFT procedure allows for the efficient deposition of binder-free Pt, Ru, and Ni NPs onto flexible polyimide films and glass surfaces at a rate of 400 mm/s. The size and quantity of the spherical NPs present on the conductive carbon surface can be tuned by adjusting the LIFT parameters such as the laser power, the scribing speed, and the source thickness. Upon increasing the laser power, the Pt NPs size decreases, and the amount of Pt in the LIFT-derived materials increases. A second laser treatment can further modulate the hydrophilicity and solvent accessibility of graphene-supported Pt NPs. Our results demonstrate that the binder-free Pt, Ru, and Ni NPs supported on few-layer graphene generated using LIFT can serve as practical, active, and robust electrocatalysts for water splitting reactions in advanced electrolyzer technology.

Introduction

Renewable energy technology holds the promise of a sustainable future. To enable efficient electrochemical conversion and utilization systems, advances in the design and preparation scheme of catalysts are necessary. Current polymer electrolyte membrane (PEM) electrolyzer technology relies on precious metals such as Pt, Rh, and Ir as catalysts.[1] Despite the scarcity of these precious metals and hence their associated high cost, Pt-group nanoparticles (NPs) are the state-of-the-art electrocatalysts for hydrogen evolution reaction (HER) occurring at the cathode of acidic electrolyzers, and transition metal NPs are used as electrocatalysts for oxygen evolution reaction (OER) at the anode of alkaline electrolyzers.[2-4] Much research effort and resources have been invested into lowering the production costs of precious-metal-based catalysts.[5,6]

Reducing the size of precious metal NPs is a strategy to achieve higher specific activity.[7] By reducing the amount of bulk Pt atoms that are not electrocatalytically active,[8] more surface Pt atoms can engage in interfacial catalysis.[2] Despite having a high atom utilization efficiency, these precious metal catalysts can be deactivated through sintering or aggregation during operation.[9] Therefore, in addition to exhibiting a high surface-to-volume ratio, NPs need to be stable during catalytic processes for practical uses.[10] Thus, new catalyst preparation strategies are needed to generate NPs that are both robust and small (in the 1-5 nm range).[11-18]

Apart from maximizing the activity and stability of the electrocatalysts, the environmental cost incurred during the synthesis process of these nanoparticle catalysts need to be considered.[19] Liquid toxic waste could be generated during the wet chemical processing steps, thereby rendering downstream post-production waste treatment cost to be higher than desirable.[20] Some of the synthesis steps may not be scalable and not compatible with a continuous flow or batch process typically used in an industrial setting.[21] From a life cycle standpoint, protocols that require wet chemicals, multiple steps, or ultra-high vacuum are not as environmentally friendly relative to a one-step dry process. Taking together the main points addressed above, the impediments to generating metal NPs as electrocatalysts for electrolyzers are: (1) low durability, (2) limited scalability, and (3) waste generation.

Here, we adapted a laser-based industrial technique to address the three above-mentioned issues related to preparing electrocatalysts. Lasers have been utilized to generate catalysts via laser ablation,[22-25] direct laser scribing,[26-29] laser pyrolysis,[30] laser-induced graphene processes,[31-34] and pulsed laser deposition or dewetting;[35-39] some of these methods require the use of liquid solvents, vacuum chambers, or high temperatures. An alternative laser-induced forward transfer (LIFT) process can serve as a one-step dry technique to generate carbon-supported metal electrocatalysts at room temperature and atmospheric pressure in a matter of seconds in a green manner.[40-43] 1064 nm laser has previously been used to turn polyimide (PI) film into a Janus graphene membrane in a one-step fashion for seawater desalination.[44] A wearable sweat sensor has been

developed using graphene prepared using the laser-induced graphene method.[45] By taking advantage of the conductivity and porosity of the LIFT-generated graphene network, a binder-free supercapacitor has been developed.[46] This low-cost LIFT method does not require an ultra-high vacuum chamber nor a high-temperature quartz tube furnace.[47] In addition to zero liquid waste being generated during the LIFT process,[48] this technique could potentially be scaled up for industrial applications by incorporating into a continuous printing or extrusion-based system.[49] In this report, finely-dispersed surfactant-free Pt NPs supported on a few-layer graphene carbon matrix are generated using the one-step LIFT technique as active and robust HER electrocatalysts (Figure 1). By tuning LIFT parameters and conditions, Pt NPs with optimized HER activity, durability, and cost are generated on flexible substrate for wearables or on hard surfaces for stationary applications. This LIFT technique was further extended to prepare Ru NPs as OER electrocatalysts. In addition to precious metal catalysts, this laser-assisted method can be applied to generate non-precious metal (NPM) Ni NPs as OER materials for use in advanced electrolyzer technology.

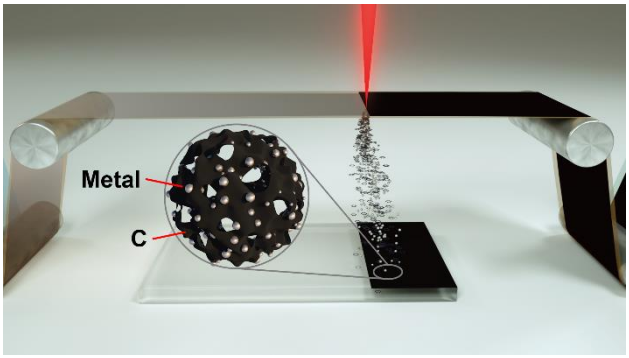

Figure 1. Using laser-induced forward transfer (LIFT) to prepare surfactant-free metal (Pt, Ru, or Ni) nanoparticles supported on a few-layer graphene carbon framework and distributed uniformly across a substrate. The substrate can be a flexible polyimide (PI) film or a rigid unmodified glass surface.

Experimental Section

Materials and Methods. Unless otherwise stated, all chemicals were purchased from commercial sources and used as received. Aqueous solutions were prepared using Milli-Q purified water (>18 MΩ cm) following published protocols.[50-52] Experiments at pH 0, 1, and 13 were performed in 1 M and 100 mM $HClO_4$ (70 wt% ACS reagent grade, Sigma-Aldrich) and in 100 mM KOH (analytical grade, Dieckmann Chemical) diluted with Milli-Q water, respectively. Solutions were sparged with N_2 (99.995% high purity grade, Linde HKO) for 30 min prior to each experiment following published methods.[53-55]

Laser-induced Forward Transfer (LIFT) Process. A DMG Lasertec 40 system equipped with a Nd:YAG 1064 nm laser operating in continuous wave (CW) mode was used for all additive manufacturing, LIFT, and scribing processes. The size and pattern of the LIFT process was pre-designed digitally and controlled by an associated computer program. Unmodified microscope glass slides (76 mm in length × 26 mm in width × 1 mm in thickness, Paul Marienfeld GmbH & Co. KG) or polyimide (PI) film (50 μm thick, Shenzhen Ze Sheng Electronic) was used as the substrate. An initial laser treatment step with a scribing speed of 400 mm/s and a laser power of 3 W was performed when electrically-insulating PI film was used as the substrate to generate a hydrophilic surface on the side irradiated by the laser beam and a hydrophobic surface on the backside of the PI film. The laser-treated electrically-conductive PI film was flipped over with the hydrophobic side facing upwards. Conductivity was measured using AC impedance and a multimeter. A layer of Pt (thickness ≈ 2 nm, 5 nm, or 10 nm), Ru (thickness ≈ 5 nm), or Ni (thickness ≈ 5 nm) on a PI film was used as the LIFT source with the Pt, Ru, or Ni side facing down, respectively. The source was placed on top of the laser-treated PI film or an unmodified glass slide. LIFT was conducted using a scribing speed between 300 mm/s and 800 mm/s with a laser power of 2 W, 3 W, or 4 W. The as-prepared LIFT-generated hydrophobic material was converted into a hydrophilic surface via a post-LIFT laser scribing step by using a scribing speed of 800 mm/s with a laser power of 0.7 W following a published procedure.[44]

Materials Characterization Methods. Transmission election microscopy (TEM) was conducted using a FEI Tecnai G2 20 S-TWIN scanning transmission electron microscope. Energy dispersive X-ray spectrometry (EDS) was performed using a JEOL model JEM-2010 transmission electron microscope. Scanning electron microscopy (SEM) was done using a Tescan MAIA3 field emission scanning electron microscope, and the images were analyzed following a published method.[56] X-ray photoemission spectroscopy (XPS) was conducted using a Thermo Scientific ESCALAB XI$^+$ X-ray photoelectron spectrometer microprobe, and the data was analyzed following a published protocol.[57] LIFT NPs were digested using the following 3-stage microwave digestion procedure with a CEM MARS microwave digestion system in 3:1 HCl: HNO_3 acidic solution.

Stage	Power (W)	Ramp (min)	Pressure (Psi)	Temp. (°C)	Hold (min)
1	280	2	70	120	5
2	280	2	80	150	15
3	Cool down (~ 30 min)				

The amount of metal in the LIFT NPs was subsequently quantified using an Agilent Technologies 7700 ICP-MS. The X-ray diffraction (XRD) measurement was collected using a Rigaku SmartLab high-resolution X-ray diffractometer. BET measurements were recorded using a Micromeritics ASAP-2020 accelerated surface area and porosimetry system. Polydispersity index (PDI) of NPs was calculated using *Eq. (1)*.[58]

$$\text{PDI for Nanoparticles} = \left(\frac{\text{Standard Deviation}}{\text{Mean Diameter}}\right)^2 \quad \text{Eq. (1)}$$

General Method for Ink Preparation. Inks were prepared following published protocols.[59] Finely ground 10 wt% Pt on Vulcan XC-72 (3.6 mg) was suspended and sonicated in EtOH (1 mL) for 20 min. The well-dispersed Pt/C slurry was treated with Nafion perfluorinated resin solution (4 μL, 5 wt% in alcohols with 15-20% water, Sigma-Aldrich). The resulting mixture was further sonicated for 10 min. This ink (10 μL) was then deposited on a glassy carbon (GC) electrode (A = 0.196 cm^2, Pine Instruments) or a laser-treated PI film (A = 1 cm^2), which was dried under a stream of N_2.

Electrochemical Experiments. Electrochemical studies were carried out using a CH Instruments 760E Electrochemical Workstation at room temperature following published procedures.[60, 61] Experiments were performed in a three-compartment cell with an aqueous "no-leak" Ag/AgCl (3 M KCl, ESA Inc.) reference electrode separated from the working electrode by a Luggin capillary as described previously.[62] Electrochemical potentials are reported relative to the reversible hydrogen electrode (RHE) using a published protocol.[63] A Pt mesh counter electrode was separated from the working electrode by a glass frit. iR compensation was conducted by measuring the solution resistance using electrochemical impedance spectroscopy (EIS) via a Bio-logic SP-150 potentiostat.[64]

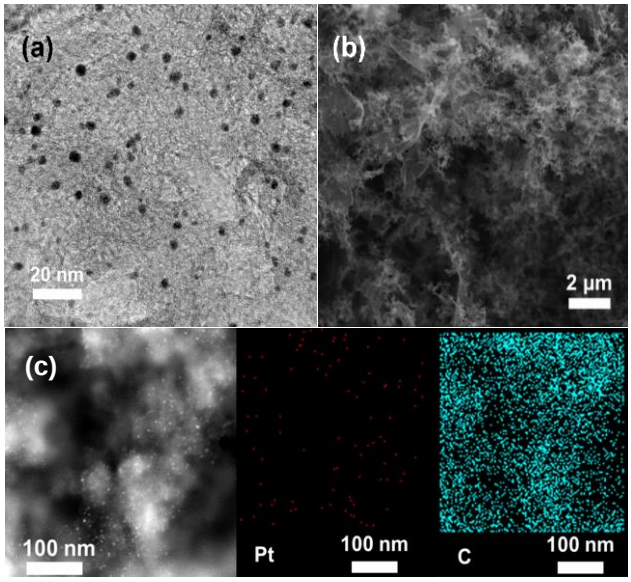

Figure 2. (a) Transmission electron microscope images, (b) scanning electron microscope images, and (c) elemental mapping of Pt NPs supported on carbon prepared using LIFT with a source thickness of 5 nm, a scribing speed of 400 mm/s, and a laser power of 3 W.

RESULTS AND DISCUSSIONS

1. Physical Characterization of Pt Nanoparticles (NPs) Prepared using a Laser-induced Forward Transfer (LIFT) Process. An industrial grade 1064 nm laser was used to generate carbon materials containing various amounts of Pt on unmodified rigid glass slides or flexible PI films via a laser induced forward transfer (LIFT) process. The resulting Pt/C construct was characterized using various physical and chemical methods. X-ray powder diffraction (XRD) was used to examine the LIFT-generated Pt/C construct on glass. XRD data show that the LIFT-generated material exhibits a diffraction pattern similar to polycrystalline Pt (Figure S1). As the power of the 1064 nm laser is increased from 2 W to 4 W, the XRD signal of the resultant Pt material decreases. As the thickness of the Pt source is decreased from 10 nm to 2 nm, the XRD signal of the resultant Pt material also decreases. A change in XRD signal could be due to a change in crystallinity, particle size, or the amount of Pt present; these possible changes will be explored further in following sections. These XRD data suggest that polycrystalline Pt structures can be generated and transferred from a Pt layer on PI to an unmodified glass surface via the LIFT process.

Transmission electron microscopy (TEM) was utilized to examine the size and shape of the Pt/C construct generated by the LIFT process. Figure 2a show that the LIFT construct contains spherical NPs and the diameter of these spherical NPs was 2.2 ± 0.4 nm with a polydispersity of 0.04. Analysis of the TEM images in Figures S2-6 show that the shape of the NPs is not affected by the laser power or the Pt source thickness. Tables S1-2 shows the effect of laser power and Pt source thickness on the size of the NPs. As the laser power increases or the Pt source thickness decreases, the size of the resulting NPs decreases (Figure 3). Scanning electron microscope (SEM) images show that the overall morphology of the Pt/C material is similar regardless of the laser power used and the Pt source thickness (Figures 2b and S7). Energy dispersive X-ray spectroscopy (EDS) was utilized to identify the chemical composition of the LIFT-generated material. Figure S8 shows that the LIFT-generated material contains Pt and C. Elemental mapping was conducted to determine the degree of aggregation of the Pt NPs. Areal scans using TEM-EDS show that Pt NPs are well-dispersed on the carbon support (Figure 2c).

Next, the Pt content in the LIFT-made carbon structure with well-dispersed Pt NPs was quantified using X-ray photoelectron spectroscopy (XPS, Figures 4a-e). Figure S9 and Tables S3-7 show the elemental analysis result. The XPS results show that the Pt NPs supported on carbon produced using LIFT contains 4.60 wt% Pt, 77.35 wt% C, 15.83 wt% O, and 2.22 wt% N (Table S4). The amount of Pt in the LIFT material increases as the laser power increases (Figure 4f) and as the source thickness increases (Figure S9). Pt was found to exist predominately as Pt in the LIFT-generated construct (Figure 4b).[65] The presence of Pt oxides does not affect HER activity because during electrocatalysis Pt oxides will be reduced to Pt *in situ* within the potential window used.[66] Figure 4c shows that the LIFT material contains C in the forms of sp^2, C-N, and C=O.[67] Figure 4d shows that the LIFT materials contain pyridinic, pyrrolic, and graphitic N.[68] These N features were previously implicated to contribute to the overall performance of electrocatalysts by serving as anchoring sites for NPs.[69] Various O species were observed in the LIFT material (Figure 4e).[70] The carbon matrix was previously observed to contain few-layer graphene features using Raman spectroscopy.[44] The porosity of the carbon structure was deduced using the BET gas adsorption-desorption method. The internal surface area of the graphene-supported Pt NPs material prepared using LIFT was found to be 170 m^2/g (Figure S10). The conductivity of LIFT Pt NPs and 10 wt% Pt on Vulcan were comparable (Table S8). Taken together, these well-dispersed Pt NPs on a conductive porous few-layer graphene support with unique N features could be beneficial for electrocatalysis.

2. Electrocatalytic Activity of Pt NPs Prepared using a LIFT Process. The electrocatalytic activity of the graphene-supported Pt NPs structure on PI is investigated. Pt is the material of choice for electrocatalytic hydrogen evolution reaction (HER) in electrolyzers.[69-72] Figures 5 and S11-18 show the linear sweep voltammograms (LSVs) of HER catalyzed using various catalysts in both acidic and basic conditions. LIFT-generated graphene-supported Pt NPs exhibits a HER onset potential of about 0 V vs. RHE at pH 0 and 13 (Figures 5a, S11, and S12), similar to state-of-the-art Pt nanoparticle HER catalysts.[2, 69-72] LIFT Pt NPs display higher HER mass and specific activities than commercial 10 wt% Pt on Vulcan XC-72 (Figures 5a, S13, S14). Control experiments with LIFT-generated graphene on PI without Pt show poor HER performance

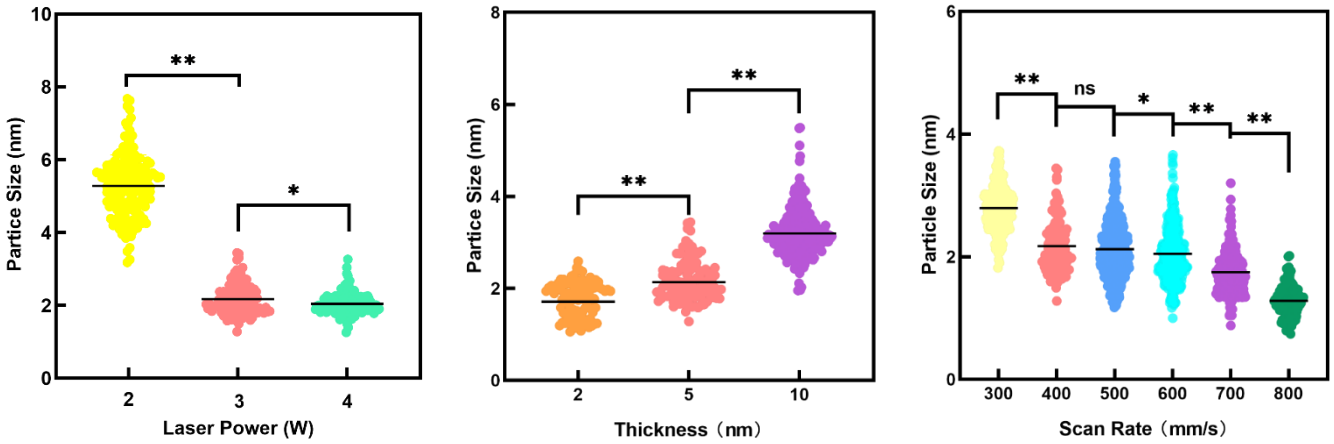

Figure 3. Particle size distribution of Pt NPs supported on carbon prepared using LIFT with (left) the laser power varying between 2 W to 4 W, (middle) the Pt source thickness varying between 2 nm to 10 nm, and (right) the scribing speed varying between 300 mm/s and 800 mm/s. **: $P \leq 0.01$, *: $P \leq 0.05$, ns: not significant.

(Figures 5a, S11, and S12: black lines), suggesting that the source of the HER activity of LIFT-generated graphene materials is from the well-dispersed Pt NPs. The graphene structure serves as a conductive matrix to supply electrons to the Pt NP active sites. Taken together, these results suggest that the LIFT-generated graphene-supported Pt NPs exhibit HER activity similar to state-of-the-art Pt-based electrocatalysts (Figures 5a, S13-S15).[69-72]

3. Factors Affecting the Performance of Pt NPs Prepared using a LIFT Process.

3.1. Thickness of Pt Layer on PI Source. To better under-stand the feature-performance relationship of these LIFT-generated Pt NPs, various parameters of the LIFT process are tuned to modulate the properties of the surfactant-free Pt NPs. Figure S17 shows the LSVs of HER catalyzed by Pt NPs prepared using different thicknesses of Pt layer on PI source used in the LIFT process. The results show that as the Pt source thickness increases from 2 nm to 5 nm, the HER activity increases. The increase in HER activity is likely due to the increase in the Pt content in the LIFT-generated materials. Upon using a 10 nm thick Pt source, the resulting Pt NPs exhibit HER activities similar to those Pt NPs generated using a 5 nm thick Pt source (Figure S17). This lack of a further increase in HER activity upon using a thicker Pt source is likely because the positive effect of increased Pt content is compensated by the negative effect of decreased surface-to-volume ratio. As the 5 nm thick Pt source uses less Pt and thus costs less relative to a 10 nm thick Pt source, the 5 nm thick Pt source is determined to exhibit the highest price-performance ratio among the various Pt on PI sources tested. These results suggest that the thickness of the Pt layer on the PI source can be used a means to optimize the size of the resulting Pt NPs embedded in the few-layer graphene matrix, thereby enhancing the resulting HER performance.

3.2. Laser Power. In addition to changing the thickness of the source, the laser power used in the LIFT process can also be adjusted to modulate the HER activity of the resulting Pt NPs. Since LIFT-generated Pt NPs using a ~5 nm thick Pt source has the best HER performance and cost-effectiveness, all subsequent optimization steps will be performed using a 5 nm thick Pt source. By increasing the laser power from 2 W to 3 W, the HER activity increases (Figures 5a and S14). The increase in activity likely stems from the increase in Pt content in the LIFT-generated material as evidenced by the increase in Pt wt% measured using XPS (Figure 4f and Tables S3-5). Upon increasing the laser power further to 4 W, the HER activity decreases (Figures 5a and S14). In short, the power of the 1064 nm laser plays an important role in determining the size and quantity of Pt NPs embedded in the few-layer graphene matrix. These results show that the electrochemical performance of the LIFT-generated Pt NPs can be optimized by tuning the LIFT parameters.

3.3. Laser Scribing Speed. To further explore the tunability of this laser-assisted nanomaterial preparation technique to make functional NPs, the scribing speed of the LIFT process was varied in an effort to modulate the irradiation dosage per unit area at a given time period. Figures S19-23 show the TEM images of Pt NPs made using LIFT at different scribing speeds. Particle size distribution analyses show that the size of the Pt NPs decreases as the scribing speed increases (Table S9). Table S10 quantifies the amount of Pt present in the LIFT NPs using XPS. As the scribing speed increases, the weight % of Pt in the LIFT NPs decreases. Taken together, the results from these two sets of experiments suggest that the size and amount of Pt in LIFT NPs can be tuned by changing the scribing speed, which is orthogonal to the other two LIFT parameters presented in 3.1 and 3.2.

3.4. Surface Hydrophilicity. Surface properties play a key role in determining the activity of electrocatalysts. The surface of the as-prepared LIFT material is hydrophobic.[44] A laser-based post-treatment was used to convert the hydrophobic surface into a hydrophilic surface.[44] Here, a similar post-LIFT laser treatment was adapted to convert the as-prepared Pt NPs supported on a hydrophobic carbon support into a hydrophilic one. The HER activity of the hydrophobic and hydrophilic Pt NPs electrocatalysts were assessed. Figure S24 shows that Pt NPs on a hydrophilic carbon support exhibits higher HER activity relative to its hydrophobic counterpart. This observation is likely due to the better wettability of the hydrophilic surface in aqueous solution, thereby boosting the accessibility of Pt NPs to H^+ in solution. This result demonstrates that by maximizing the number of Pt NPs in contact with solution, the electrocatalytic activity of LIFT-generated Pt NPs can be enhanced.

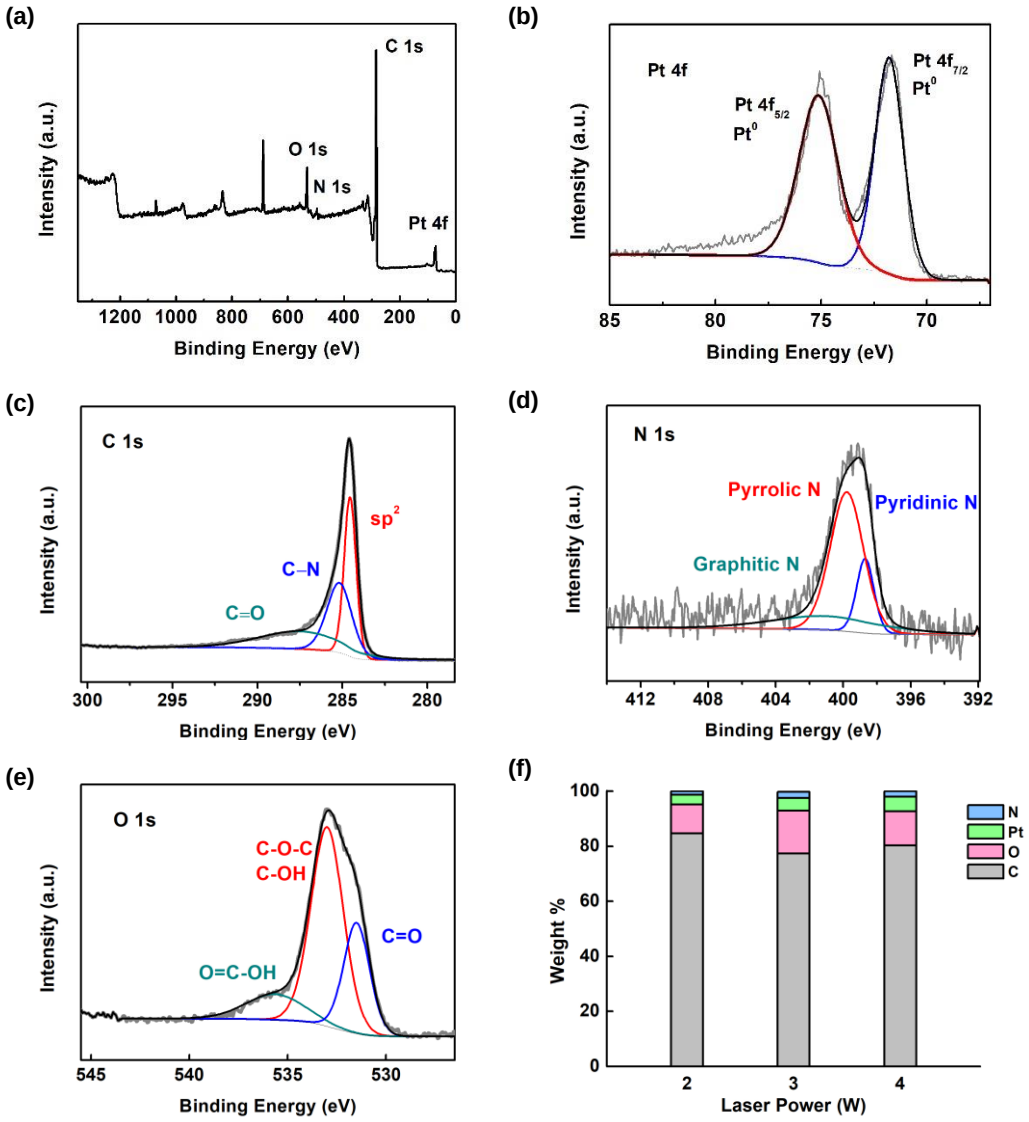

Figure 4. X-ray photoelectron spectroscopy (XPS) chemical composition analysis of Pt nanoparticles supported on carbon prepared using LIFT with a laser power of 3 W. (a) XPS survey spectrum of LIFT Pt/C. High-resolution XPS (b) Pt 4f, (c) C 1s, (d) N 1s, and (e) O 1s spectra of LIFT Pt/C. Gray = measured XPS spectra, blue/red/turquoise = individual fit components, black = cumulative sum of individual fit components. (f) XPS elemental analysis of Pt/C prepared using LIFT with the laser power varying between 2 W to 4 W.

4. Durability of Pt NPs Prepared using a LIFT Process. Pt NPs produced using a LIFT process with a 5 nm thick Pt source, a laser power of 3 W, a scribing speed of 400 mm/s, and a post-LIFT laser treatment to generate a hydrophilic surface exhibit the highest HER activity among the conditions tested. To examine if the Pt NPs catalysts are suitable for practical uses, the robustness of the graphene-supported Pt NPs catalyst is monitored. Two types of long-term stability tests were conducted. First, the potential at which the catalyst can sustain a reductive current density of 5 mA/cm^2 was monitored as a function of time. The chronopotentiometry data shown in Figure S25 demonstrates that the Pt NPs catalyst is stable for 24 hours in pH 0. At pH 13, the Pt NPs on graphene on PI exhibits a decrease in HER activity after 6 hours of operation because the PI substrate decomposes under basic conditions. The observation of the long lifetime of the catalyst at pH 0 could be explained by the presence of the few-layer graphene carbon framework that could serve as anchoring sites for the Pt NPs to prevent agglomeration.

A second long-term ON-OFF-ON cycling test was conducted in pH 0 (Figures 5b and S26). In the first ON cycle, the Pt NPs catalyst was first cycled between +0.424 and -1.376 V vs. RHE for 2912 times at a scan rate of 100 mV/s. The Pt NPs catalyst was then soaked in the pH 0 solution for 10 hours under open circuit potential condition to simulate an idling period. The same Pt NPs catalyst was further subjected to another 2912 cycles in the second ON cycle. Minimal decrease in HER activity was observed after the whole accelerated durability measurement, suggesting that the Pt NPs catalyst is stable at pH 0 under industry-relevant operating conditions. These results corroborate that Pt NPs supported on graphene generated using LIFT is more stable than state-of-the-art Pt electrocatalysts prepared using other methods under HER operating conditions.[28, 71-74]

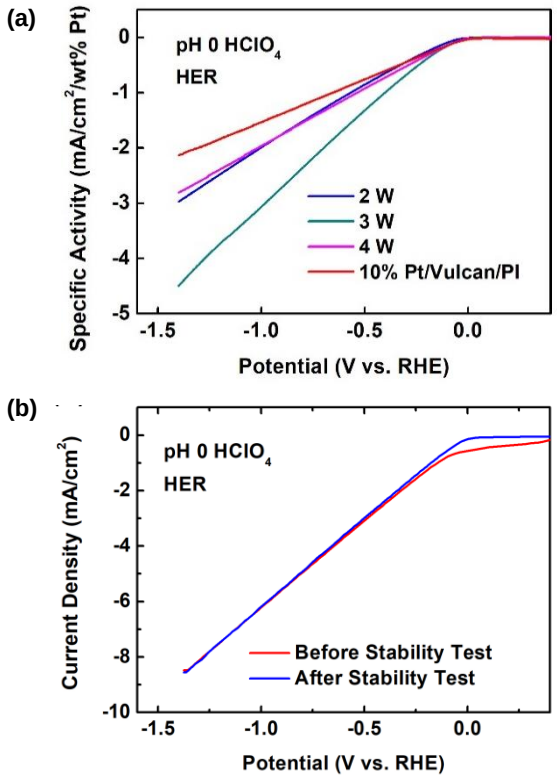

Figure 5. (a) Specific HER activity of Pt nanoparticles supported on carbon prepared using LIFT with a source thickness of 5 nm, a scribing speed of 400 mm/s, and a laser power of 2 W (blue), 3 W (turquoise), and 4 W (magenta), and 10 wt% commercial Pt/C sample (red) in N_2-saturated pH 0 $HClO_4$ (1 M) with a scan rate of 10 mV/s. (b) Linear sweep voltammograms (LSVs) of Pt NPs supported on carbon prepared using LIFT with a source thickness of 5 nm, a scribing speed of 400 mm/s, and a laser power of 3 W in N_2-saturated pH 0 $HClO_4$ (1 M) at a scan rate of 10 mV/s before (red) and after (blue) cycling for 2912 times at a scan rate of 100 mV/s, followed by soaking for 10 h in N_2-saturated pH 0 $HClO_4$ (1 M) under open circuit potential with no current passing through the working electrode, then cycling for another 2912 times.

5. Broader Applications of the LIFT Technology.

5.1. Using LIFT to Prepare Ru NPs for Oxygen Evolution Reaction.

This one-step laser-assisted nanomaterials fabrication method was further exploited to generate NPs that can address reactions more complex than HER. OER electrocatalysis was chosen to be the next target reaction. Previous studies have found that Ru is a cheaper alternative to Ir as OER catalysts under acidic conditions.[75,76] LIFT was then used to prepare Ru NPs supported on few-layer graphene using a 5 nm thick Ru source on PI, a scribing speed of 400 mm/s, and a laser power of 3 W. Figure S27 shows the TEM image of LIFT Ru NPs and the electrochemical performance of Ru NPs toward OER electrocatalysis in pH 1 $HClO_4$. LIFT Ru NPs reach 2 mA/cm^2·μg Ru with an OER overpotential of 214 mV, a value similar to previously reported Ru electrocatalysts.[75,76] The amount of Ru in the LIFT NPs was quantified by ICP-MS to be 0.15 μg. These results corroborate that LIFT can be used as a new technique to prepare OER catalysts for acidic electrolyzers.

5.2. Utilizing LIFT to Prepare Non-precious Metal (NPM) Ni NPs.

In addition to preparing precious metal catalysts, the possibility of using this room-temperature synthetic procedure to generate non-precious metal (NPM) NPs was tested. Previous reports showed that Ni was a candidate material with decent OER performance under alkaline conditions. Here, Ni NPs were prepared using LIFT with a 5 nm thick Ni substrate on PI, a scribing speed of 400 mm/s, and a laser power of 3 W. Figure S28 shows the TEM image, XPS spectra, and LSV of LIFT Ni NPs. Composition analyses show that these LIFT NPs contain 4.89 wt% Ni. LIFT Ni NPs exhibit an anodic wave at ca. 1.5 V vs. RHE, akin to the oxidation signal typically observed in Ni OER materials.[64] The electrochemical activity of LIFT Ni NPs in pH 14 KOH. LIFT Ni NPs reached an OER current density of 1 mA/cm^2 with an overpotential of 269 mV, a value similar to other reported Ni nanomaterials.[64] These results suggest that LIFT can be used as a greener, cheaper, and more efficient alternative to fabricate NPM NPs with OER activity comparable to known Ni catalysts.

6. Benefits of Producing Electrocatalysts using the LIFT Strategy.

Unlike solution processable methods to make metal NPs where chemical reductants and solvents have to be used and disposed of, the LIFT process only requires a laser system that can be reused. Unlike other physical or chemical vacuum deposition processes, the LIFT procedure can be conducted in air under ambient condition, which drastically saves initial plant construction costs and ongoing production costs. Since no liquid waste is generated throughout the whole LIFT procedure to produce surfactant-free Pt, Ru, and Ni NPs supported on a few-layer graphene carbon support, this LIFT protocol is regarded as an environmental-friendly method for electrocatalyst synthesis and is therefore highly desirable by the green chemical industry. This LIFT technique can in principle be extended to generate catalytically-active NPs containing other non-precious metals (NPM) and transition metal alloys. Apart from using flexible PI as a substrate, rigid glass slide can also be used to capture the LIFT-generated NPs. In addition to the flexibility in the range of substrates that can be used, Nafion is not needed as a binder to adhere catalysts onto a surface for activity testing using a 3-electrode setup. This feature saves time and money for high-throughput screening of catalysts. The acidic sulfonate groups of Nafion might affect the catalyst's intrinsic catalytic activity and product selectivity by binding to the surface of the catalyst of interest. With the use of a laser system, patterning is also possible. This maskless writing function allows for future device to be fabricated with more functionality without the need to use a template. A second laser processing step can also be incorporated to change the hydrophobic carbon matrix into a hydrophilic carbon matrix.[44] Another benefit of using the LIFT method is the potential for continuous fabrication of electrocatalyst films, which can be adapted into a scalable industrial process.

Table 1. Tuning the size and loading of NPs to improve their catalytic activity by altering various key parameters of the LIFT process.

Parameter	Loading	Size
Power (W) ↑	↑	↓
Thickness (nm) ↑	↑	↑
Scribing Speed (mm/s) ↑	↓	↓

Conclusions

Current limitations in the field of renewable energy include the challenge in preparing electrocatalysts with (1) high durability, (2) high scalability, and (3) low waste generation. In this report, an industrial laser scribing machine was repurposed to prepare electrocatalysts using a laser-induced forward transfer (LIFT) method without the use of any wet chemicals under room temperature and ambient pressure with zero liquid waste generation. Through the use of this dry processing technique, non-aggregated Pt, Ru, or Ni NPs in the size range of 1-5 nm were randomly dispersed onto a PI film surface and supported on a few-layer graphene carbon matrix. The size of NPs has been demonstrated previously to affect the catalytic activity of NPs.[77, 78] With a versatile and tunable LIFT method at hand to generate surfactant-free metal NPs in a facile manner, various parameters including source thickness, laser power, and scribing speed were tuned to optimize the size and quantity of the Pt NPs in an effort to maximize their catalytic activity (Table 1). This additive LIFT technique can decouple the effect of laser power, scribing speed, and source thickness on the loading and size of resultant NPs through repeatedly applying LIFT at the same location to produce larger quantities of NPs without changing their sizes. Well-dispersed Pt NPs supported on graphene produced using a source thickness of 5 nm and a laser power of 3 W exhibit the most active hydrogen evolution reaction (HER) catalysts among the LIFT materials screened. This graphene-supported catalyst contains 4.6 wt% Pt, and the diameter of the well-dispersed spherical Pt NPs was ca. 2.2 nm. The binder-free Pt NPs supported on carbon catalyst maintains an onset potential of -39 mV vs. RHE even after over 5800 on-off cycles or 24 h of uninterrupted operation at a reductive current density of 5 mA/cm^2 under strongly acidic conditions. A post-LIFT laser treatment can further adjust the hydrophobicity/hydrophilicity of the laser-scribed electrocatalytic materials with remarkable durability to open new doors for a wide range of applications. This laser-assisted approach can be extended to produce Ru and non-precious Ni NPs as OER electrocatalysts for use in next-generation electrolyzers.

ASSOCIATED CONTENT

Supporting Information. Supplemental Figures S1-28, Supplemental Tables S1-10, and additional information including XRD data, TEM images, SEM images, BET results, cyclic voltammograms, and chronopotentiometry data as discussed in the text. This material is available free of charge via the Internet at http://pubs.acs.org.

AUTHOR INFORMATION

Corresponding Author

* Authors to whom correspondence should be addressed:
E-mail: *kc.chan@polyu.edu.hk (KCC) and *ecmtse@hku.hk (ECMT)

Notes

There are no conflicts of interest to declare.

ACKNOWLEDGMENT

E.C.M.T. would like to express our gratitude to the Croucher Foundation for a start-up fund and the Hung Hing Ying Physical Sciences Research Fund for supporting our research activities. X.M. would like to thank Frankie Y.F. Chan at the Electron Microscope Unit (EMU) at the University of Hong Kong (HKU) for his help with materials characterization and Dr. Dongxue Han for her help with sputter deposition. We thank Dr. Guijun Mitch Li for his insights. We would like to recognize Jenkin C. K. Tsui and Professor Kwong Yu Chan for their help with BET measurements.

REFERENCES

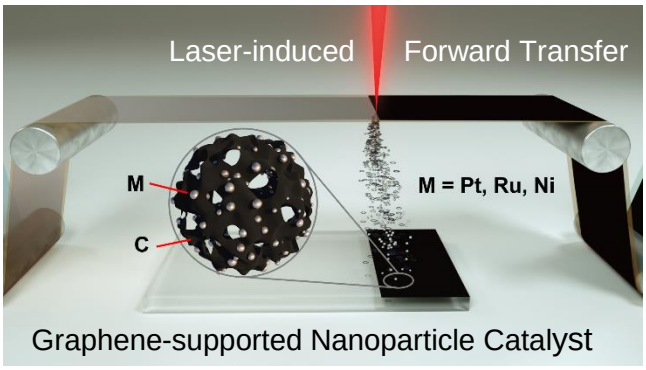

Synopsis

Robust graphene-supported nano-electrocatalysts can be deposited onto rigid/flexible substrates via a facile laser-assisted process without liquid waste generation.

1. Stamenkovic, V. R.; Strmcnik, D.; Lopes, P. P.; Markovic, N. M., Energy and fuels from electrochemical interfaces. *Nat. Mater.* **2016,** 16, 57.
2. Cheng, N.; Stambula, S.; Wang, D.; Banis, M. N.; Liu, J.; Riese, A.; Xiao, B.; Li, R.; Sham, T.-K.; Liu, L.-M.; Botton, G. A.; Sun, X., Platinum single-atom and cluster catalysis of the hydrogen evolution reaction. *Nat. Commun.* **2016,** 7, 13638.
3. Yin, H.; Zhao, S.; Zhao, K.; Muqsit, A.; Tang, H.; Chang, L.; Zhao, H.; Gao, Y.; Tang, Z., Ultrathin platinum nanowires grown on single-layered nickel hydroxide with high hydrogen evolution activity. *Nat. Commun.* **2015,** 6, 6430.
4. Chen, Z.; Higgins, D.; Yu, A.; Zhang, L.; Zhang, J., A review on non-precious metal electrocatalysts for PEM fuel cells. *Energy Environ. Sci.* **2011,** 4, (9), 3167-3192.
5. Zeng, M.; Li, Y., Recent advances in heterogeneous electrocatalysts for the hydrogen evolution reaction. *J. Mater. Chem. A* **2015,** 3, (29), 14942-14962.
6. Zalitis, C. M.; Kucernak, A. R.; Sharman, J.; Wright, E., Design principles for platinum nanoparticles catalysing electrochemical hydrogen evolution and oxidation reactions: edges are much more active than facets. *J. Mater. Chem. A* **2017,** 5, (44), 23328-23338.
7. Yang, X.-F.; Wang, A.; Qiao, B.; Li, J.; Liu, J.; Zhang, T., Single-Atom Catalysts: A New Frontier in Heterogeneous Catalysis. *Acc. Chem. Res.* **2013,** 46, (8), 1740-1748.
8. Stephens, I. E. L.; Chorkendorff, I., Minimizing the Use of Platinum in Hydrogen-Evolving Electrodes. *Angew. Chem. Int. Ed.* **2011,** 50, (7), 1476-1477.
9. Shao-Horn, Y.; Sheng, W. C.; Chen, S.; Ferreira, P. J.; Holby, E. F.; Morgan, D., Instability of Supported Platinum Nanoparticles in Low-Temperature Fuel Cells. *Top. Catal.* **2007,** 46, (3), 285-305.
10. Wu, J.; Yuan, X. Z.; Martin, J. J.; Wang, H.; Zhang, J.; Shen, J.; Wu, S.; Merida, W., A review of PEM fuel cell durability: Degradation mechanisms and mitigation strategies. *J. Power Sources* **2008,** 184, (1), 104-119.
11. Li, S.; Cheng, C.; Sagaltchik, A.; Pachfule, P.; Zhao, C.; Thomas, A., Metal-Organic Precursor–Derived Mesoporous Carbon Spheres with Homogeneously Distributed Molybdenum Carbide/Nitride Nanoparticles for Efficient Hydrogen Evolution in Alkaline Media. *Adv. Funct. Mater.* **2019,** 29, (3), 1807419.

12. Liu, G.; Eichelsdoerfer, D. J.; Rasin, B.; Zhou, Y.; Brown, K. A.; Liao, X.; Mirkin, C. A., Delineating the pathways for the site-directed synthesis of individual nanoparticles on surfaces. *Proc. Natl. Acad. Sci. USA* **2013,** 110, (3), 887-891.
13. Huang, J.; Mensi, M.; Oveisi, E.; Mantella, V.; Buonsanti, R., Structural Sensitivities in Bimetallic Catalysts for Electrochemical CO2 Reduction Revealed by Ag–Cu Nanodimers. *J. Am. Chem. Soc.* **2019,** 141, (6), 2490-2499.
14. Huang, J.; Hörmann, N.; Oveisi, E.; Loiudice, A.; De Gregorio, G. L.; Andreussi, O.; Marzari, N.; Buonsanti, R., Potential-induced nanoclustering of metallic catalysts during electrochemical CO2 reduction. *Nat. Commun.* **2018,** 9, (1), 3117.
15. Kalisman, P.; Nakibli, Y.; Amirav, L., Perfect Photon-to-Hydrogen Conversion Efficiency. *Nano Lett.* **2016,** 16, (3), 1776-1781.
16. Liu, G.; Young, K. L.; Liao, X.; Personick, M. L.; Mirkin, C. A., Anisotropic Nanoparticles as Shape-Directing Catalysts for the Chemical Etching of Silicon. *J. Am. Chem. Soc.* **2013,** 135, (33), 12196-12199.
17. Beckers, N. A.; Huynh, S.; Zhang, X.; Luber, E. J.; Buriak, J. M., Screening of Heterogeneous Multimetallic Nanoparticle Catalysts Supported on Metal Oxides for Mono-, Poly-, and Heteroaromatic Hydrogenation Activity. *ACS Catal.* **2012,** 2, (8), 1524-1534.
18. Zhu, Q.-L.; Xu, Q., Immobilization of Ultrafine Metal Nanoparticles to High-Surface-Area Materials and Their Catalytic Applications. *Chem* **2016,** 1, (2), 220-245.
19. Stavis, S. M.; Fagan, J. A.; Stopa, M.; Liddle, J. A., Nanoparticle Manufacturing – Heterogeneity through Processes to Products. *ACS Appl. Nano Mater.* **2018,** 1, (9), 4358-4385.
20. Dahl, J. A.; Maddux, B. L. S.; Hutchison, J. E., Toward Greener Nanosynthesis. *Chem. Rev.* **2007,** 107, (6), 2228-2269.
21. Hutchison, J. E., The Road to Sustainable Nanotechnology: Challenges, Progress and Opportunities. *ACS Sustain. Chem. Eng.* **2016,** 4, (11), 5907-5914.
22. Hunter, B. M.; Blakemore, J. D.; Deimund, M.; Gray, H. B.; Winkler, J. R.; Müller, A. M., Highly Active Mixed-Metal Nanosheet Water Oxidation Catalysts Made by Pulsed-Laser Ablation in Liquids. *J. Am. Chem. Soc.* **2014,** 136, (38), 13118-13121.
23. Blakemore, J. D.; Gray, H. B.; Winkler, J. R.; Müller, A. M., Co3O4 Nanoparticle Water-Oxidation Catalysts Made by Pulsed-Laser Ablation in Liquids. *ACS Catal.* **2013,** 3, (11), 2497-2500.
24. Amendola, V.; Meneghetti, M., Laser ablation synthesis in solution and size manipulation of noble metal nanoparticles. *Phys. Chem. Chem. Phys.* **2009,** 11, (20), 3805-3821.
25. Torres-Mendieta, R.; Ventura-Espinosa, D.; Sabater, S.; Lancis, J.; Mínguez-Vega, G.; Mata, J. A., In situ decoration of graphene sheets with gold nanoparticles synthetized by pulsed laser ablation in liquids. *Sci. Rep.* **2016,** 6, 30478.
26. El-Kady, M. F.; Strong, V.; Dubin, S.; Kaner, R. B., Laser Scribing of High-Performance and Flexible Graphene-Based Electrochemical Capacitors. *Science* **2012,** 335, (6074), 1326-1330.
27. Gao, W.; Singh, N.; Song, L.; Liu, Z.; Reddy, A. L. M.; Ci, L.; Vajtai, R.; Zhang, Q.; Wei, B.; Ajayan, P. M., Direct laser writing of micro-supercapacitors on hydrated graphite oxide films. *Nat. Nanotechnol.* **2011,** 6, 496.
28. Nayak, P.; Jiang, Q.; Kurra, N.; Wang, X.; Buttner, U.; Alshareef, H. N., Monolithic laser scribed graphene scaffolds with atomic layer deposited platinum for the hydrogen evolution reaction. *J. Mater. Chem. A* **2017,** 5, (38), 20422-20427.
29. Chrisey, D. B., The Power of Direct Writing. *Science* **2000,** 289, (5481), 879-881.
30. Sourice, J.; Quinsac, A.; Leconte, Y.; Sublemontier, O.; Porcher, W.; Haon, C.; Bordes, A.; De Vito, E.; Boulineau, A.; Jouanneau Si Larbi, S.; Herlin-Boime, N.; Reynaud, C., One-Step Synthesis of Si@C Nanoparticles by Laser Pyrolysis: High-Capacity Anode Material for Lithium-Ion Batteries. *ACS Appl. Mater. Interfaces* **2015,** 7, (12), 6637-6644.
31. Ye, R.; James, D. K.; Tour, J. M., Laser-Induced Graphene: From Discovery to Translation. *Adv. Mater.* **2019,** 31, (1), 1803621.

32. Han, X.; Ye, R.; Chyan, Y.; Wang, T.; Zhang, C.; Shi, L.; Zhang, T.; Zhao, Y.; Tour, J. M., Laser-Induced Graphene from Wood Impregnated with Metal Salts and Use in Electrocatalysis. *ACS Appl. Nano Mater.* **2018,** 1, (9), 5053-5061.
33. Zhang, J.; Ren, M.; Li, Y.; Tour, J. M., In Situ Synthesis of Efficient Water Oxidation Catalysts in Laser-Induced Graphene. *ACS Energy Lett.* **2018,** 3, (3), 677-683.
34. Zhang, J.; Zhang, C.; Sha, J.; Fei, H.; Li, Y.; Tour, J. M., Efficient Water-Splitting Electrodes Based on Laser-Induced Graphene. *ACS Appl. Mater. Interfaces* **2017,** 9, (32), 26840-26847.
35. Sacré, N.; Duca, M.; Garbarino, S.; Imbeault, R.; Wang, A.; Hadj Youssef, A.; Galipaud, J.; Hufnagel, G.; Ruediger, A.; Roué, L.; Guay, D., Tuning Pt–Ir Interactions for NH3 Electrocatalysis. *ACS Catal.* **2018,** 8, (3), 2508-2518.
36. Temmel, S. E.; Fabbri, E.; Pergolesi, D.; Lippert, T.; Schmidt, T. J., Investigating the Role of Strain toward the Oxygen Reduction Activity on Model Thin Film Pt Catalysts. *ACS Catal.* **2016,** 6, (11), 7566-7576.
37. Gawande, M. B.; Goswami, A.; Felpin, F.-X.; Asefa, T.; Huang, X.; Silva, R.; Zou, X.; Zboril, R.; Varma, R. S., Cu and Cu-Based Nanoparticles: Synthesis and Applications in Catalysis. *Chem. Rev.* **2016,** 116, (6), 3722-3811.
38. Mróz, W.; Budner, B.; Tokarz, W.; Piela, P.; Korwin-Pawlowski, M. L., Ultra-low-loading pulsed-laser-deposited platinum catalyst films for polymer electrolyte membrane fuel cells. *J. Power Sources* **2015,** 273, 885-893.
39. Owusu-Ansah, E.; Horwood, C. A.; El-Sayed, H. A.; Birss, V. I.; Shi, Y. J., A method for the formation of Pt metal nanoparticle arrays using nanosecond pulsed laser dewetting. *Appl. Phys. Lett.* **2015,** 106, (20), 203103.
40. Esrom, H.; Zhang, J.-Y.; Kogelschatz, U.; Pedraza, A. J., New approach of a laser-induced forward transfer for deposition of patterned thin metal films. *Appl. Surf. Sci.* **1995,** 86, (1), 202-207.
41. Bohandy, J.; Kim, B. F.; Adrian, F. J.; Jette, A. N., Metal deposition at 532 nm using a laser transfer technique. *J. Appl. Phys.* **1988,** 63, (4), 1158-1162.
42. Bohandy, J.; Kim, B. F.; Adrian, F. J., Metal deposition from a supported metal film using an excimer laser. *J. Appl. Phys.* **1986,** 60, (4), 1538-1539.
43. Braudy, R. S., Laser writing. *Proc. IEEE* **1969,** 57, (10), 1771-1772.
44. Li, G.; Law, W.-C.; Chan, K. C., Floating, highly efficient, and scalable graphene membranes for seawater desalination using solar energy. *Green Chem.* **2018,** 20, (16), 3689-3695.
45. Li, G.; Mo, X.; Law, W.-C.; Chan, K. C., Wearable Fluid Capture Devices for Electrochemical Sensing of Sweat. *ACS Appl. Mater. Interfaces* **2019,** 11, (1), 238-243.
46. Li, G.; Mo, X.; Law, W.-C.; Chan, K. C., 3D Printed Graphene/Nickel Electrodes for High Areal Capacitance Electrochemical Storage. *J. Mater. Chem. A* **2019,** 7, 4055-4062.
47. Li, G.; Meng, Z.; Qian, J.; Ho, C.-L.; Lau, S. P.; Wong, W.-Y.; Yan, F., Inkjet printed pseudocapacitive electrodes on laser-induced graphene for electrochemical energy storage. *Mater. Today Energy* **2019,** 12, 155-160.
48. Toulemonde, M.; Muller, J. C.; Stuck, B., Transfer of a Metal From a Transparent Film to the Surface of Silicon to Produce P-N Junction Solar Cells. *J. Sol. Energy Eng.* **1986,** 108, (2), 102-104.
49. Serra, P.; Piqué, A., Laser-Induced Forward Transfer: Fundamentals and Applications. *Adv. Mater. Technol.* **2019,** 4, (1), 1800099.
50. Barile, C. J.; Tse, E. C. M.; Li, Y.; Sobyra, T. B.; Zimmerman, S. C.; Hosseini, A.; Gewirth, A. A., Proton switch for modulating oxygen reduction by a copper electrocatalyst embedded in a hybrid bilayer membrane. *Nat. Mater.* **2014,** 13, (6), 619-623.
51. Gautam, R. P.; Lee, Y. T.; Herman, G. L.; Moreno, C. M.; Tse, E. C. M.; Barile, C. J., Controlling Proton and Electron Transfer Rates to Enhance the Activity of an Oxygen Reduction Electrocatalyst. *Angew. Chem. Int. Ed.* **2018,** 57, (41), 13480-13483.
52. Li, Y.; Tse, E. C. M.; Barile, C. J.; Gewirth, A. A.; Zimmerman, S. C., Photoresponsive Molecular Switch for Regulating Transmembrane Proton-Transfer Kinetics. *J. Am. Chem. Soc.* **2015,** 137, (44), 14059-14062.

53. Tse, E. C. M.; Barile, C. J.; Gewargis, J. P.; Li, Y.; Zimmerman, S. C.; Gewirth, A. A., Anion Transport through Lipids in a Hybrid Bilayer Membrane. *Anal. Chem.* **2015,** 87, (4), 2403-2409.
54. Tse, E. C. M.; Barile, C. J.; Li, Y.; Zimmerman, S. C.; Hosseini, A.; Gewirth, A. A., Proton transfer dynamics dictate quinone speciation at lipid-modified electrodes. *Phys. Chem. Chem. Phys.* **2017,** 19, (10), 7086-7093.
55. Supakul, S. N.; Barile, C. J., Membrane-Modified Metal Triazole Complexes for the Electrocatalytic Reduction of Oxygen and Carbon Dioxide. *Front. Chem.* **2018,** 6, 543.
56. Tse, E. C. M.; Gewirth, A. A., Effect of Temperature and Pressure on the Kinetics of the Oxygen Reduction Reaction. *J. Phys. Chem. A* **2015,** 119, (8), 1246-1255.
57. Varnell, J. A.; Tse, E. C. M.; Schulz, C. E.; Fister, T. T.; Haasch, R. T.; Timoshenko, J.; Frenkel, A. I.; Gewirth, A. A., Identification of carbon-encapsulated iron nanoparticles as active species in non-precious metal oxygen reduction catalysts. *Nat. Commun.* **2016,** 7, 12582.
58. Clayton, K. N.; Salameh, J. W.; Wereley, S. T.; Kinzer-Ursem, T. L., Physical characterization of nanoparticle size and surface modification using particle scattering diffusometry. *Biomicrofluidics* **2016,** 10, (5), 054107.
59. Tse, E. C. M.; Schilter, D.; Gray, D. L.; Rauchfuss, T. B.; Gewirth, A. A., Multicopper Models for the Laccase Active Site: Effect of Nuclearity on Electrocatalytic Oxygen Reduction. *Inorg. Chem.* **2014,** 53, (16), 8505-8516.
60. Barile, C. J.; Tse, E. C. M.; Li, Y.; Gewargis, J. P.; Kirchschlager, N. A.; Zimmerman, S. C.; Gewirth, A. A., The Flip-Flop Diffusion Mechanism across Lipids in a Hybrid Bilayer Membrane. *Biophys. J.* **2016,** 110, (11), 2451-2462.
61. Tse, E. C. M.; Barile, C. J.; Kirchschlager, N. A.; Li, Y.; Gewargis, J. P.; Zimmerman, S. C.; Hosseini, A.; Gewirth, A. A., Proton transfer dynamics control the mechanism of O2 reduction by a non-precious metal electrocatalyst. *Nat. Mater.* **2016,** 15, (7), 754-759.
62. Thorseth, M. A.; Letko, C. S.; Tse, E. C. M.; Rauchfuss, T. B.; Gewirth, A. A., Ligand Effects on the Overpotential for Dioxygen Reduction by Tris(2-pyridylmethyl)amine Derivatives. *Inorg. Chem.* **2013,** 52, (2), 628-634.
63. Tse, E. C. M.; Varnell, J. A.; Hoang, T. T. H.; Gewirth, A. A., Elucidating Proton Involvement in the Rate-Determining Step for Pt/Pd-Based and Non-Precious-Metal Oxygen Reduction Reaction Catalysts Using the Kinetic Isotope Effect. *J. Phys. Chem. Lett.* **2016,** 7, (18), 3542-3547.
64. Tse, E. C. M.; Hoang, T. T. H.; Varnell, J. A.; Gewirth, A. A., Observation of an Inverse Kinetic Isotope Effect in Oxygen Evolution Electrochemistry. *ACS Catal.* **2016,** 6, (9), 5706-5714.
65. Wang, G.; Parrondo, J.; He, C.; Li, Y.; Ramani, V., Pt/C/Ni(OH)2 Bi-Functional Electrocatalyst for Enhanced Hydrogen Evolution Reaction Activity under Alkaline Conditions. *J. Electrochem. Soc.* **2017,** 164, (13), F1307-F1315.
66. Gilroy, D.; Conway, B. E., Surface oxidation and reduction of platinum electrodes: Coverage, kinetic and hysteresis studies. *Can. J. Chem.* **1968,** 46, (6), 875-890.
67. Zhang, L.; Wang, X.; Wang, R.; Hong, M., Structural Evolution from Metal–Organic Framework to Hybrids of Nitrogen-Doped Porous Carbon and Carbon Nanotubes for Enhanced Oxygen Reduction Activity. *Chem. Mater.* **2015,** 27, (22), 7610-7618.
68. Wang, M.; Wu, Z.; Dai, L., Graphitic carbon nitrides supported by nitrogen-doped graphene as efficient metal-free electrocatalysts for oxygen reduction. *J. Electroanal. Chem.* **2015,** 753, 16-20.
69. Zhang, H.; An, P.; Zhou, W.; Guan, B. Y.; Zhang, P.; Dong, J.; Lou, X. W., Dynamic traction of lattice-confined platinum atoms into mesoporous carbon matrix for hydrogen evolution reaction. *Sci. Adv.* **2018,** 4, (1), eaao6657.
70. Yu, Y.-H.; Lin, Y.-Y.; Lin, C.-H.; Chan, C.-C.; Huang, Y.-C., High-performance polystyrene/graphene-based nanocomposites with excellent anti-corrosion properties. *Polym. Chem.* **2014,** 5, (2), 535-550.
71. Zhang, H.; Ren, W.; Guan, C.; Cheng, C., Pt decorated 3D vertical graphene nanosheet arrays for efficient methanol oxidation and hydrogen evolution reactions. *J. Mater. Chem. A* **2017,** 5, (41), 22004-22011.

72. Yan, X.; Li, H.; Sun, J.; Liu, P.; Zhang, H.; Xu, B.; Guo, J., Pt nanoparticles decorated high-defective graphene nanospheres as highly efficient catalysts for the hydrogen evolution reaction. *Carbon* **2018,** 137, 405-410.
73. Ghanim, A. H.; Koonce, J. G.; Hasa, B.; Rassoolkhani, A. M.; Cheng, W.; Peate, D. W.; Lee, J.; Mubeen, S., Low-Loading of Pt Nanoparticles on 3D Carbon Foam Support for Highly Active and Stable Hydrogen Production. *Front. Chem.* **2018,** 6, 523.
74. Shang, X.; Liu, Z.-Z.; Lu, S.-S.; Dong, B.; Chi, J.-Q.; Qin, J.-F.; Liu, X.; Chai, Y.-M.; Liu, C.-G., Pt–C Interfaces Based on Electronegativity-Functionalized Hollow Carbon Spheres for Highly Efficient Hydrogen Evolution. *ACS Appl. Mater. Interfaces* **2018,** 10, (50), 43561-43569.
75. Reier, T.; Oezaslan, M.; Strasser, P., Electrocatalytic Oxygen Evolution Reaction (OER) on Ru, Ir, and Pt Catalysts: A Comparative Study of Nanoparticles and Bulk Materials. *ACS Catal.* **2012,** 2, (8), 1765-1772.
76. Paoli, E. A.; Masini, F.; Frydendal, R.; Deiana, D.; Schlaup, C.; Malizia, M.; Hansen, T. W.; Horch, S.; Stephens, I. E. L.; Chorkendorff, I., Oxygen evolution on well-characterized mass-selected Ru and RuO2 nanoparticles. *Chem. Sci.* **2015,** 6, (1), 190-196.
77. Yano, H.; Watanabe, M.; Iiyama, A.; Uchida, H., Particle-size effect of Pt cathode catalysts on durability in fuel cells. *Nano Energy* **2016,** 29, 323-333.
78. Tan, T. L.; Wang, L.-L.; Zhang, J.; Johnson, D. D.; Bai, K., Platinum Nanoparticle During Electrochemical Hydrogen Evolution: Adsorbate Distribution, Active Reaction Species, and Size Effect. *ACS Catal.* **2015,** 5, (4), 2376-2383.

Supporting Information (SI) for:

A Scalable Laser-assisted Method to Produce Active and Robust Graphene-supported Nanoparticle Electrocatalysts

Xiaoyong Mo,[1] Kang-Cheung Chan,[2, *] and Edmund C. M. Tse[1, *]

[1] Department of Chemistry, University of Hong Kong, Pokfulam Road, Hong Kong SAR, PRC

[2] Advanced Manufacturing Technology Research Centre, Department of Industrial and Systems Engineering, Hong Kong Polytechnic University, Hung Hom, Hong Kong SAR, PRC

[*] Authors to whom correspondence should be addressed:

E-mail: [*]kc.chan@polyu.edu.hk (KCC) and [*]ecmtse@hku.hk (ECMT)

Supplemental Figures S1-28 and Supplemental Tables S1-9 contain information including XRD data, TEM images, SEM images, BET results, cyclic voltammograms, and chronopotentiometry data as discussed in the main text.

Supplemental Figures

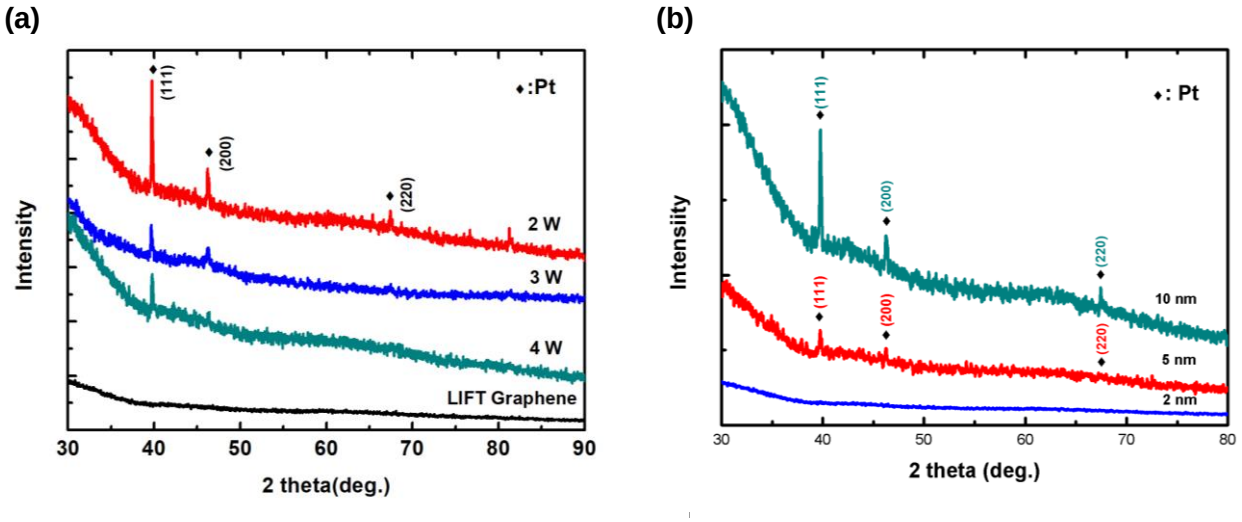

Figure S1. X-ray diffraction (XRD) spectra of Pt nanoparticles (NPs) supported on a few-layer graphene carbon prepared using a facile laser-induced forward transfer (LIFT) method with (a) a Pt source thickness of 5 nm and a laser power of 2 W (red), 3 W (blue), 4 W (turquoise), and a glass substrate as the background signal (black), and (b) a laser power of 3 W and a Pt source thickness of 2 nm (blue), 5 nm (red), and 10 nm (turquoise). The presence of Pt oxide signal in the X-ray photoelectron spectroscopy (XPS) results presented in Figure 4b could be because XPS is a surface sensitive technique, therefore the surface Pt oxide signal is more pronounced than the Pt signal originating from the interior of the NPs. The absence of Pt oxides signal in the XRD spectra in Figure S1 could be due to the amorphous nature of the Pt oxide skin. From a performance standpoint, the presence of Pt oxides does not affect HER activity because during electrocatalysis Pt oxides will be reduced *in situ* to Pt within the potential window used.

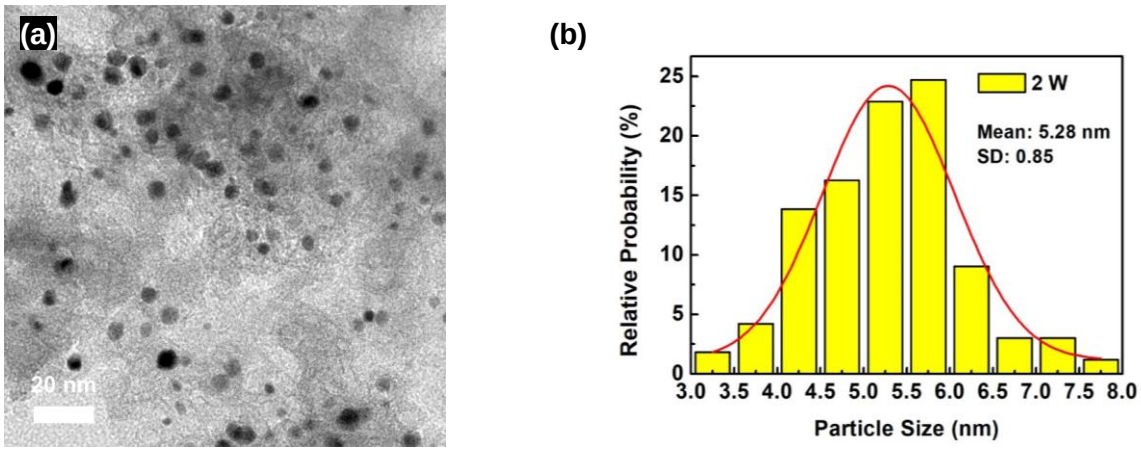

Figure S2. (a) Transmission electron microscope (TEM) image and (b) particle size distribution analysis of Pt NPs supported on a few-layer graphene carbon network prepared using a LIFT process with a Pt source thickness of 5 nm, a scribing speed of 400 mm/s, and a laser power of 2 W.

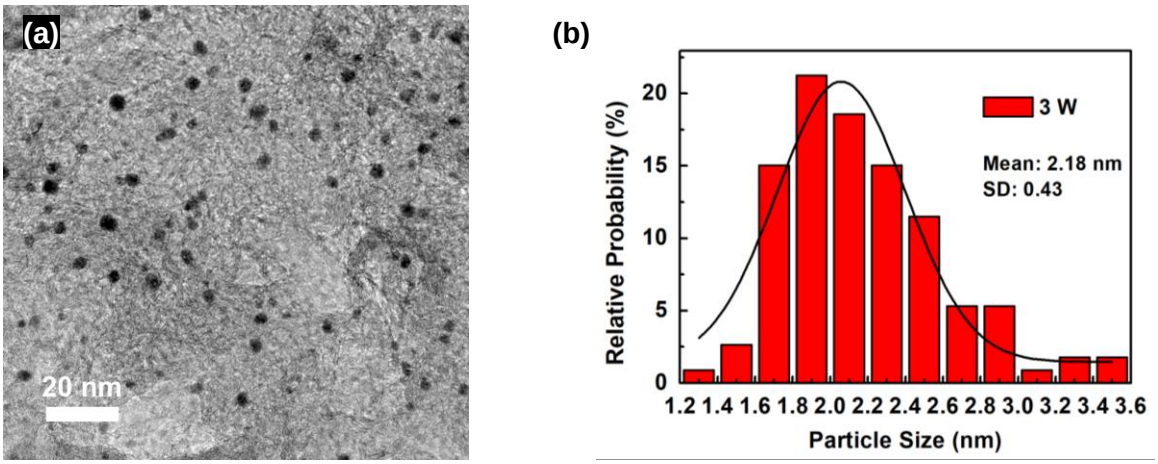

Figure S3. (a) TEM image and (b) particle size distribution analysis of Pt NPs supported on a few-layer graphene carbon network prepared using a LIFT process with a Pt source thickness of 5 nm, a scribing speed of 400 mm/s, and a laser power of 3 W.

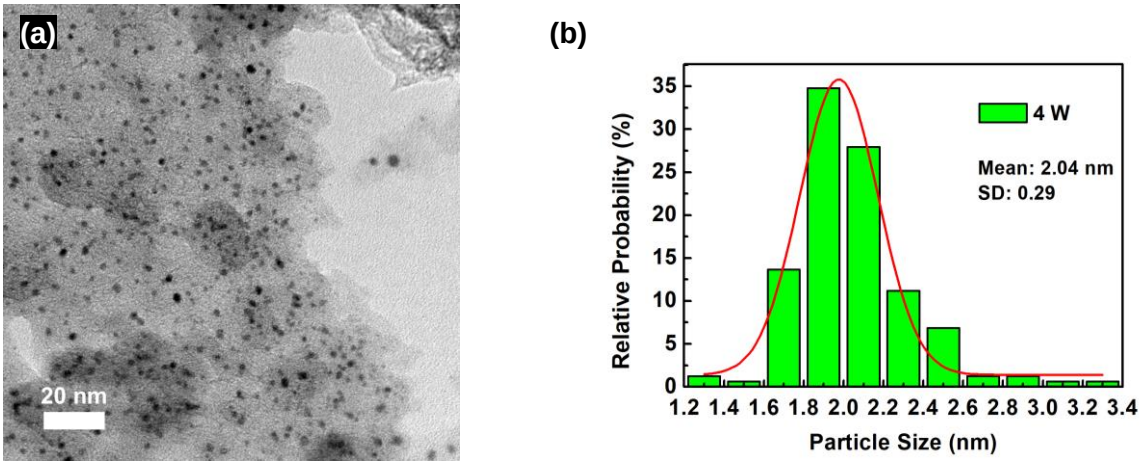

Figure S4. (a) TEM image and (b) particle size distribution analysis of Pt NPs supported on a few-layer graphene carbon network prepared using a LIFT process with a Pt source thickness of 5 nm, a scribing speed of 400 mm/s, and a laser power of 4 W.

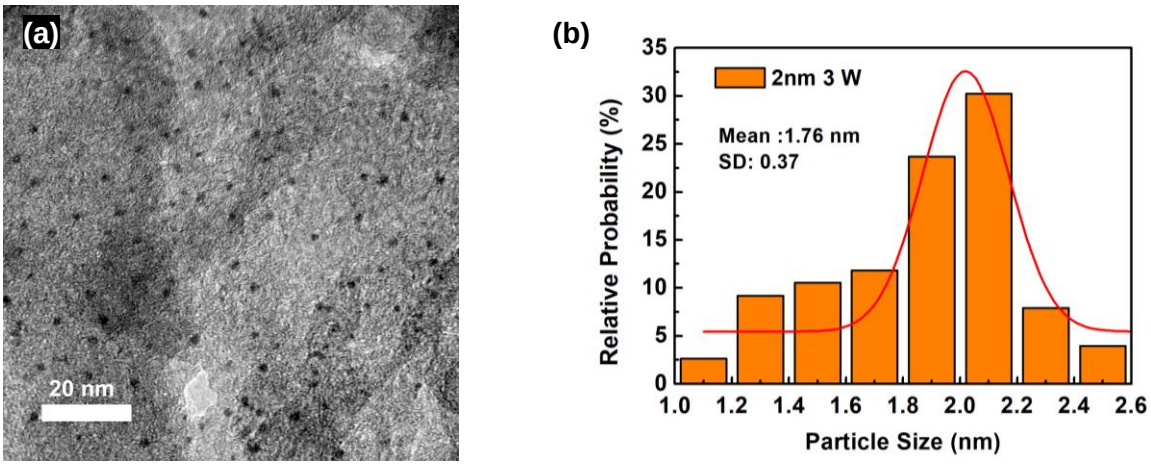

Figure S5. (a) TEM image and (b) particle size distribution analysis of Pt NPs supported on a few-layer graphene carbon network prepared using a LIFT process with a scribing speed of 400 mm/s, a laser power of 3 W, and a Pt source thickness of 2 nm.

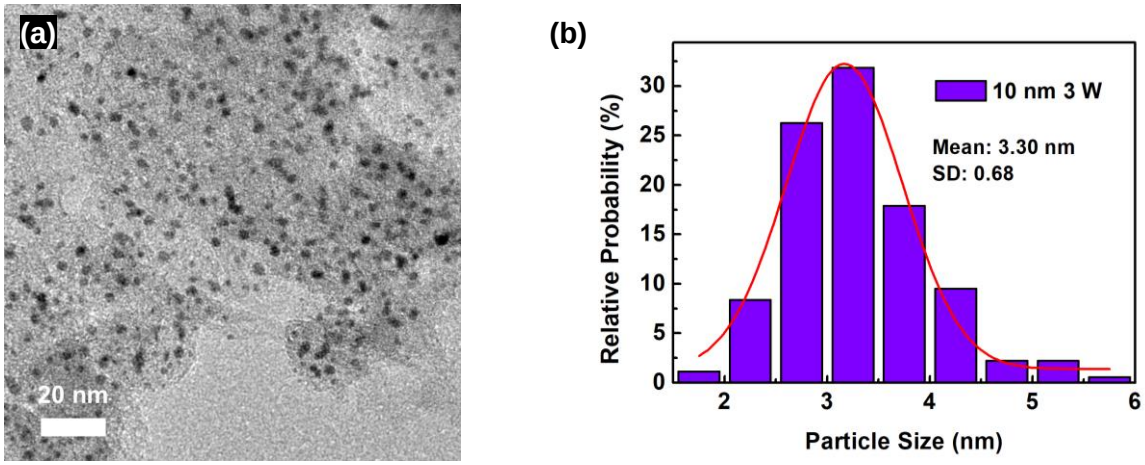

Figure S6. (a) TEM image and (b) particle size distribution analysis of Pt NPs supported on a few-layer graphene carbon network prepared using a LIFT process with a laser power of 3 W, and a scribing speed of 400 mm/s, and a Pt source thickness of 10 nm.

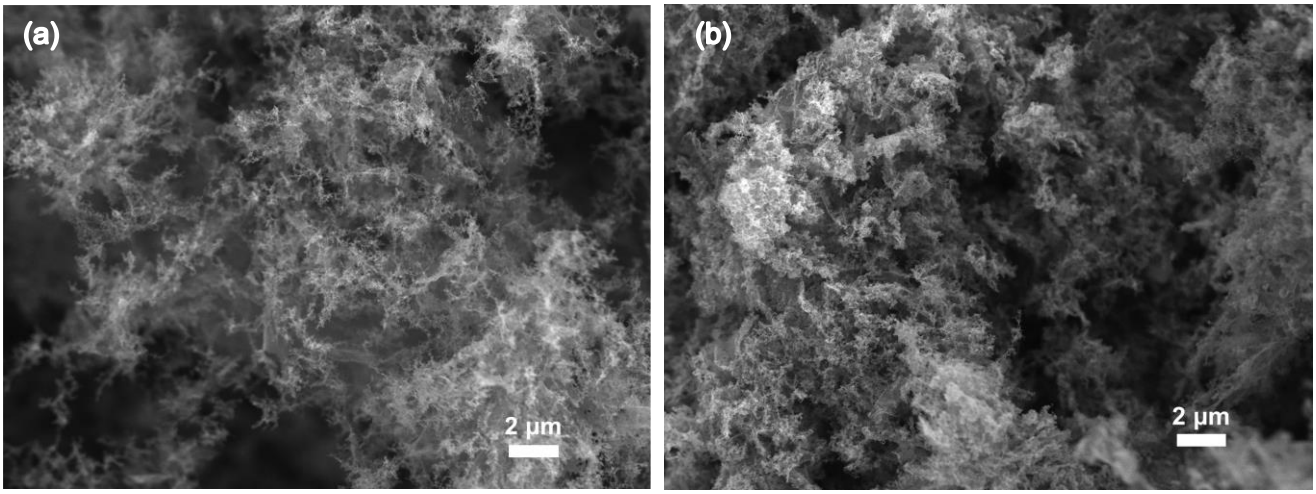

Figure S7. Scanning electron microscope (SEM) images of Pt NPs supported on a few-layer graphene carbon prepared using LIFT with a laser power of 3 W, a scribing speed of 400 mm/s, and a Pt source thickness of (a) 2 nm and (b) 10 nm.

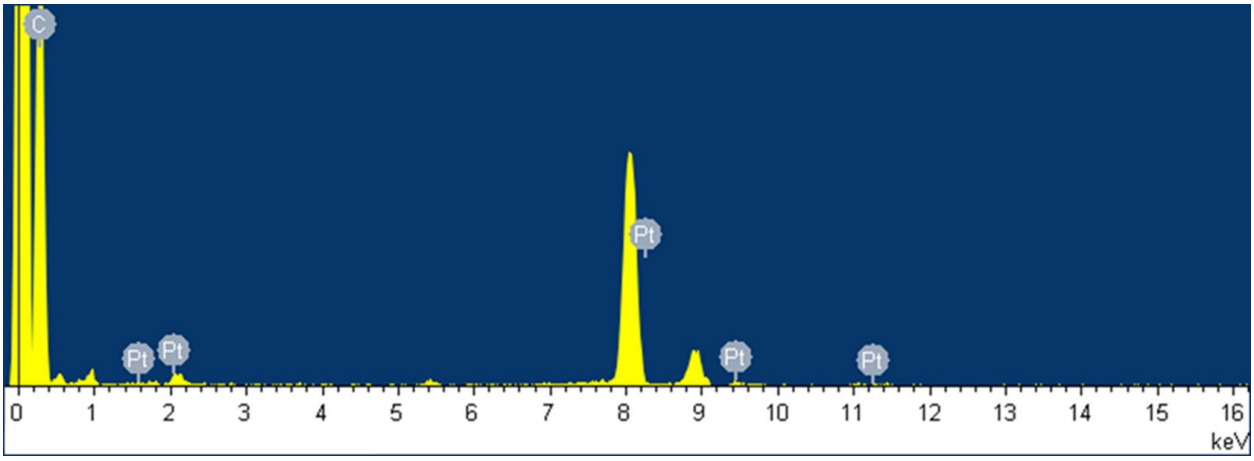

Figure S8. Energy dispersive X-ray spectroscopy (EDS) sum spectrum of Pt NPs supported on a few-layer graphene carbon prepared using LIFT with a Pt source thickness of 5 nm, a scribing speed of 400 mm/s, and a laser power of 3 W.

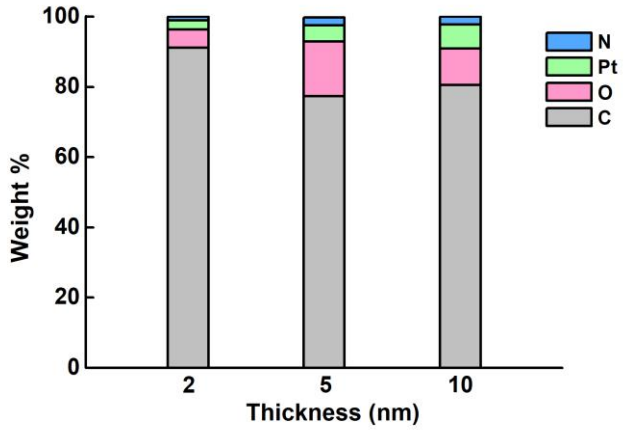

Figure S9. XPS elemental analysis of Pt/C prepared using LIFT with the source thickness varying between 2 nm and 10 nm.

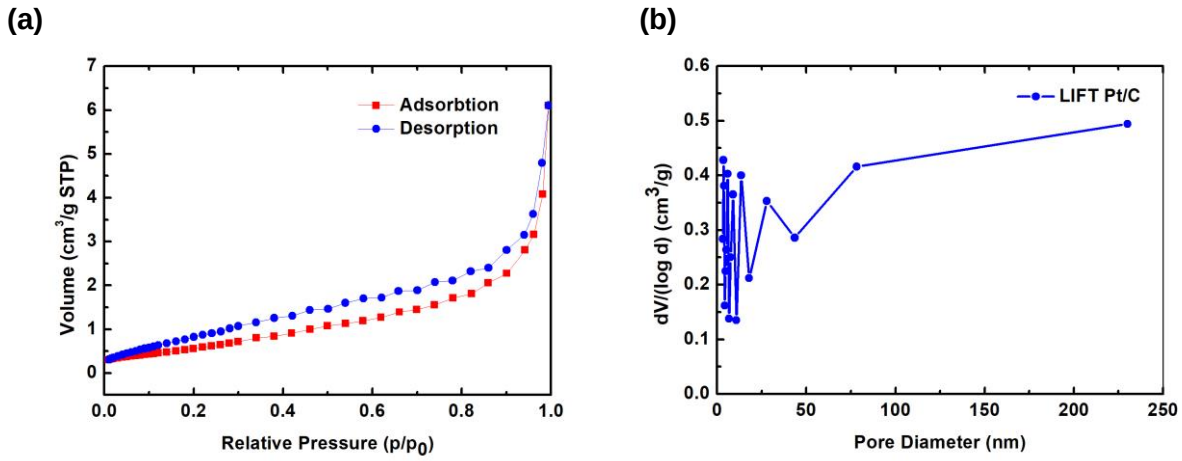

Figure S10. (a) Gas adsorption-desorption BET isotherms and (b) pore size distribution measurements of Pt NPs supported on a few-layer graphene carbon prepared using LIFT with a Pt source thickness of 5 nm, a scribing speed of 400 mm/s, and a laser power of 3 W.

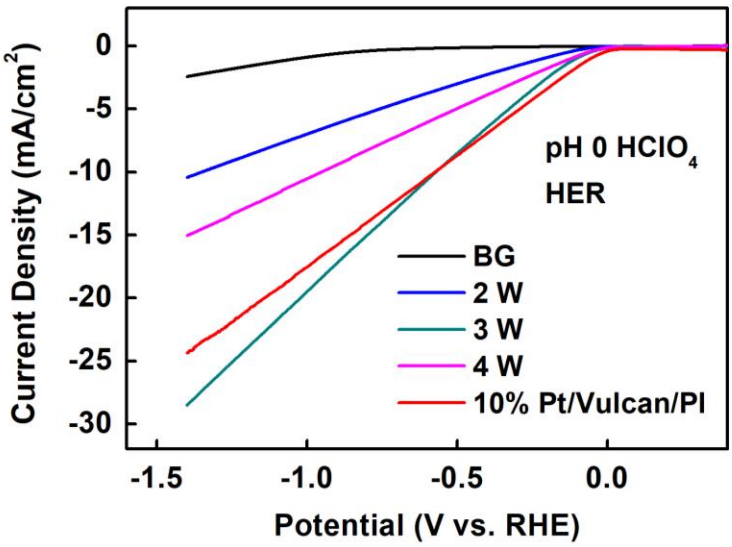

Figure S11. Linear sweep voltammograms (LSVs) of Pt NPs supported on carbon prepared using LIFT with a source thickness of 5 nm and (a) a laser power of 2 W (blue), 3 W (turquoise), and 4 W (magenta), and 10 wt% commercial Pt/C sample (red) in N_2-saturated pH 0 $HClO_4$ (1 M) with a scan rate of 10 mV/s,

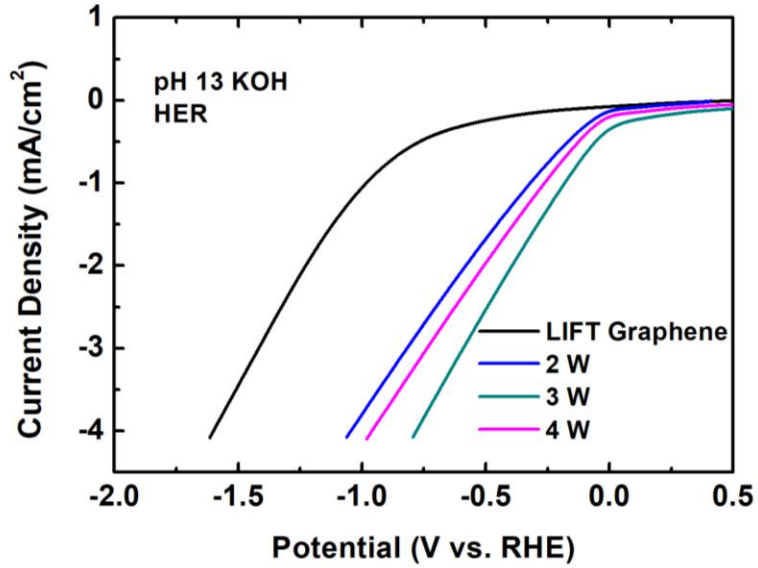

Figure S12. LSVs of Pt NPs supported on carbon prepared using LIFT with a source thickness of 5 nm, a scribing speed of 400 mm/s, and a laser power of 2 W (blue), 3 W (turquoise), and 4 W (magenta), and LIFT graphene without Pt (black) in N_2-saturated pH 13 KOH (100 mM) with a scan rate of 10 mV/s.

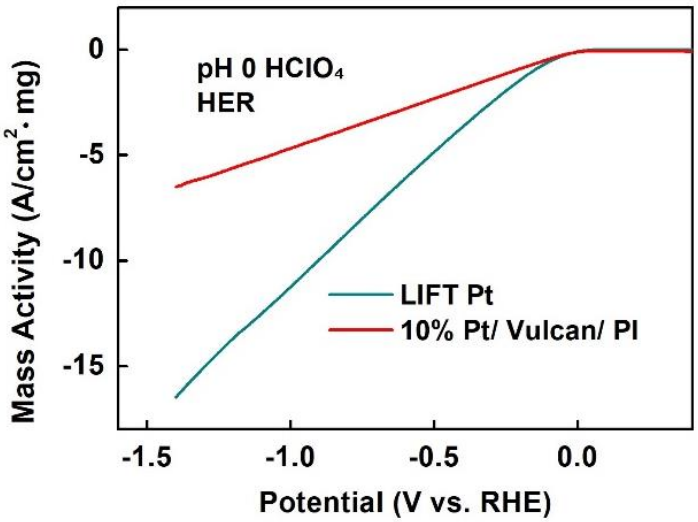

Figure S13. HER mass activity of Pt NPs supported on carbon prepared using LIFT with a source thickness of 5 nm, a scribing speed of 400 mm/s, and a laser power of 3 W (turquoise), and 10 wt% commercial Pt/C sample (red) in N_2-saturated pH 0 $HClO_4$ (1 M) with a scan rate of 10 mV/s.

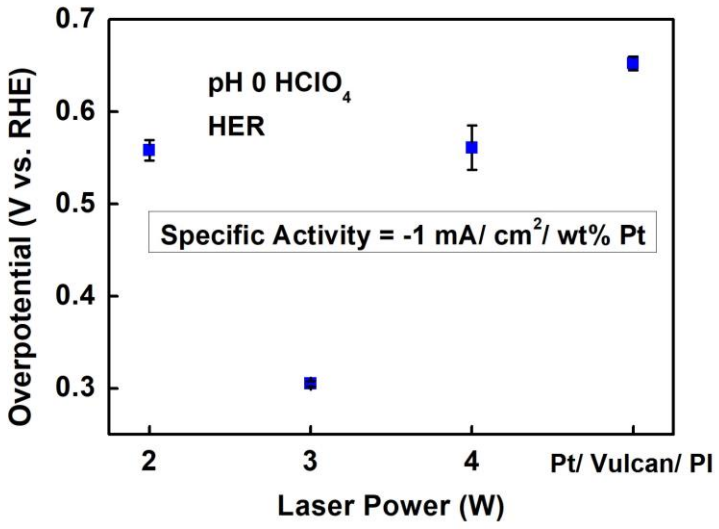

Figure S14. Plot of overpotentials needed to achieve a HER specific activity of -1 mA/cm^2/wt% Pt of Pt NPs supported on carbon prepared using LIFT with a source thickness of 5 nm, a scribing speed of 400 mm/s, and a laser power of 2, 3, and 4 W, and 10 wt% commercial Pt/C sample in N_2-saturated pH 0 $HClO_4$ (1 M) with a scan rate of 10 mV/s. The results show that Pt NPs generated using LIFT with a laser power of 3 W (with 4.6 wt% Pt) exhibits enhanced HER performance in terms of HER specific activity as compared to that of commercial 10wt% Pt on Vulcan XC-72.

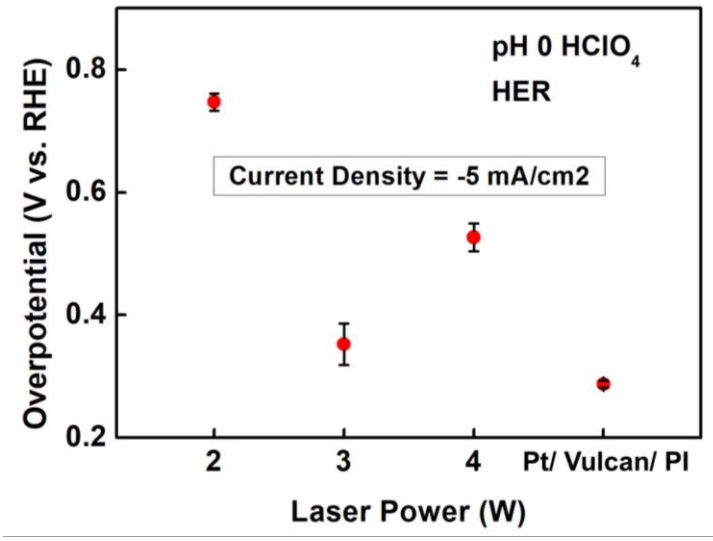

Figure S15. Plot of overpotentials needed to achieve a HER current density of -5 mA/cm^2 of Pt NPs supported on carbon prepared using LIFT with a source thickness of 5 nm, a scribing speed of 400 mm/s, and a laser power of 2, 3, and 4 W in N_2-saturated pH 0 $HClO_4$ (1 M) with a scan rate of 10 mV/s. The results show that Pt NPs generated using LIFT with a laser power of 3 W (with 4.6 wt% Pt) exhibits HER performance in terms of HER current density similar to that of commercial 10wt% Pt on Vulcan XC-72.

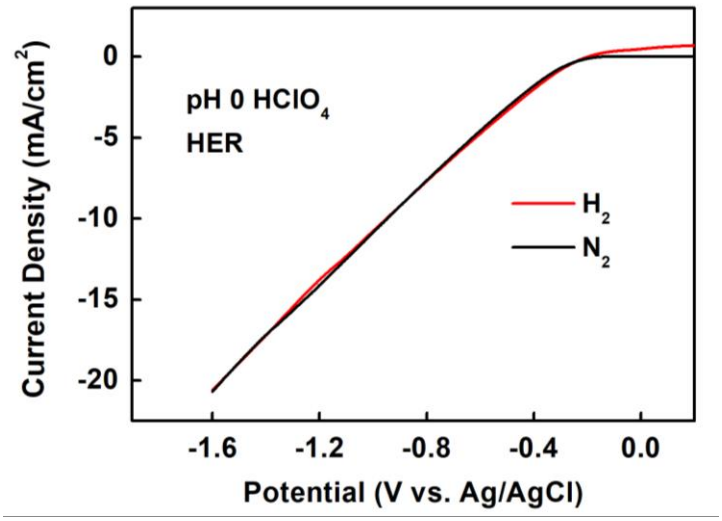

Figure S16. LSVs of Pt NPs (1.26 μg Pt/cm^2) supported on carbon prepared using LIFT with a source thickness of 5 nm, a scribing speed of 400 mm/s, and a laser power of 3 W in N_2-saturated (black) and H_2-saturated (red) pH 0 $HClO_4$ (1 M) with a scan rate of 10 mV/s. The results show that the presence of H_2 does not change the performance of the electrocatalyst. The results also show that the reference potential does not drift or change when switching from a N_2 to a H_2 atmosphere.

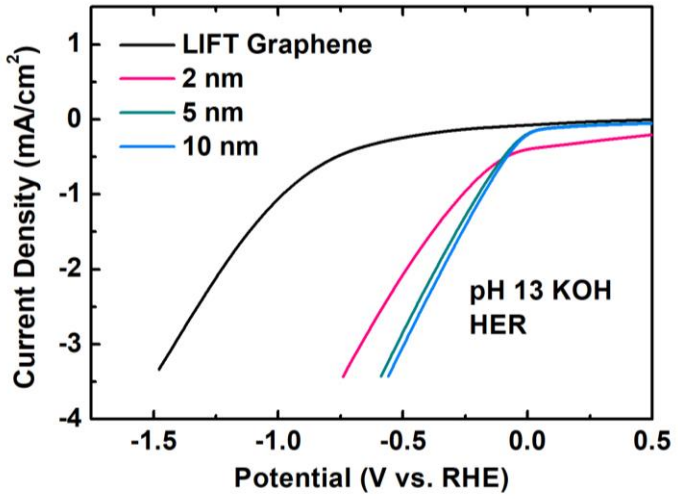

Figure S17. LSVs of Pt NPs supported on carbon prepared using LIFT with a laser power of 3 W, a scribing speed of 400 mm/s, and a source thickness of 2 nm (magenta), 5 nm (turquoise), and 10 nm (blue), and LIFT graphene without Pt (black) in N_2-saturated pH 13 KOH (100 mM) with a scan rate of 10 mV/s.

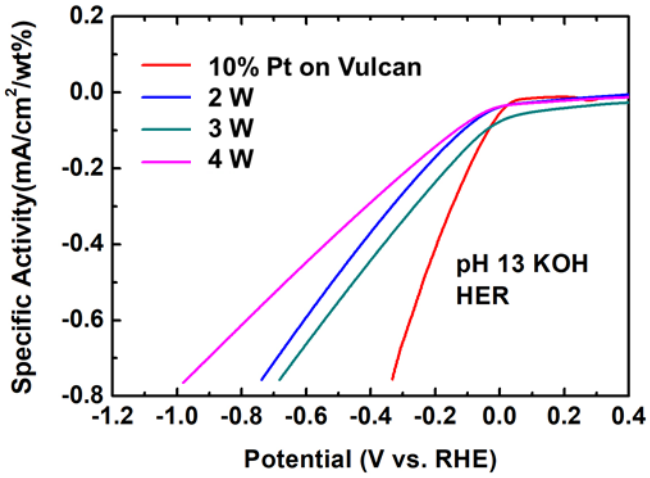

Figure S18. Specific HER activity of Pt NPs supported on carbon prepared using LIFT with a source thickness of 5 nm, a scribing speed of 400 mm/s, and a laser power of 2 W (blue), 3 W (turquoise), and 4 W (magenta), and 10 wt% commercial Pt/C sample (red) in N_2-saturated pH 13 KOH (100 mM) with a scan rate of 10 mV/s.

The difference in specific activity between the LIFT Pt/C and commercial Pt/C observed in Figure S18 is likely due to the different sample preparation methods. Nafion was used as a binder for the commercial Pt/C case, but no binder was used for the LIFT-generated Pt/C case.

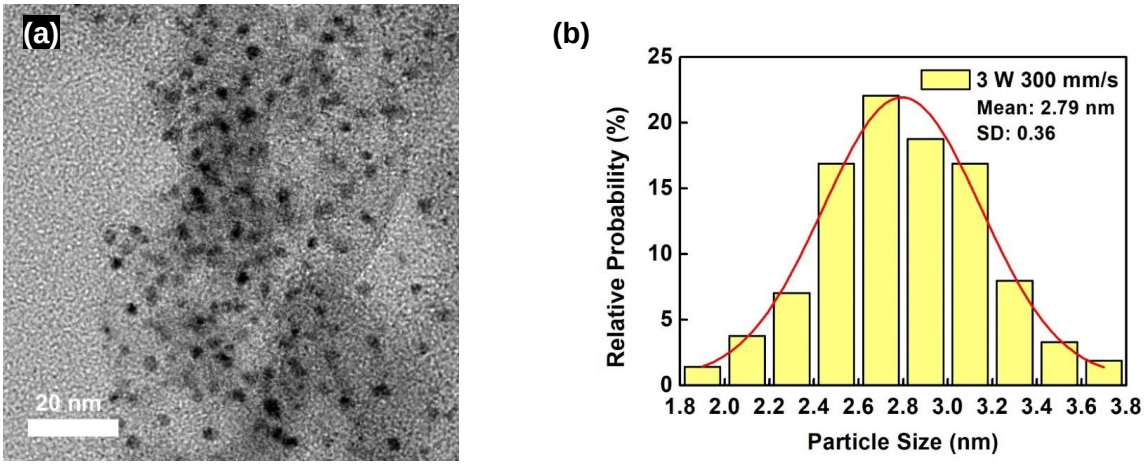

Figure S19. (a) TEM image and (b) particle size distribution analysis of Pt NPs supported on a few-layer graphene carbon network prepared using a LIFT process with a Pt source thickness of 5 nm, a laser power of 3 W, and a scribing speed of 300 mm/s.

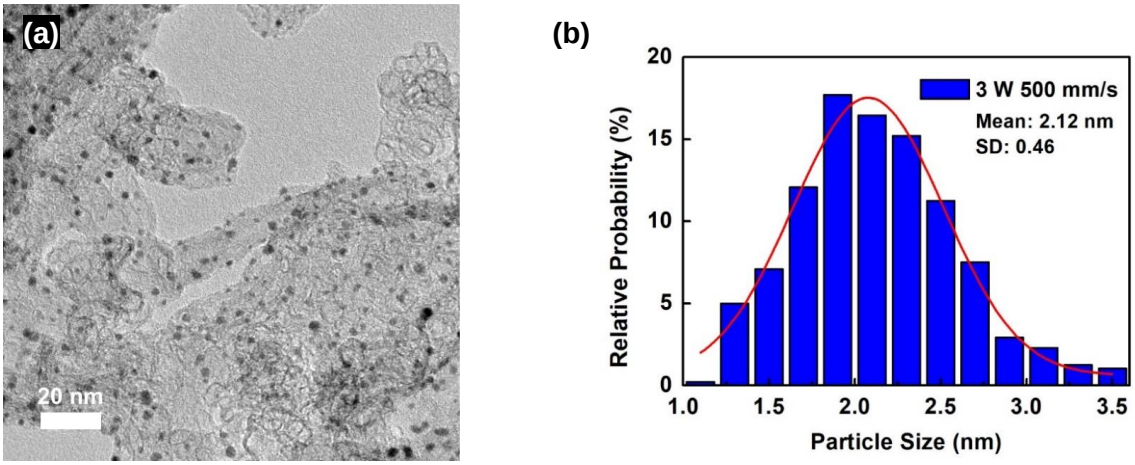

Figure S20. (a) TEM image and (b) particle size distribution analysis of Pt NPs supported on a few-layer graphene carbon network prepared using a LIFT process with a Pt source thickness of 5 nm, a laser power of 3 W, and a scribing speed of 500 mm/s.

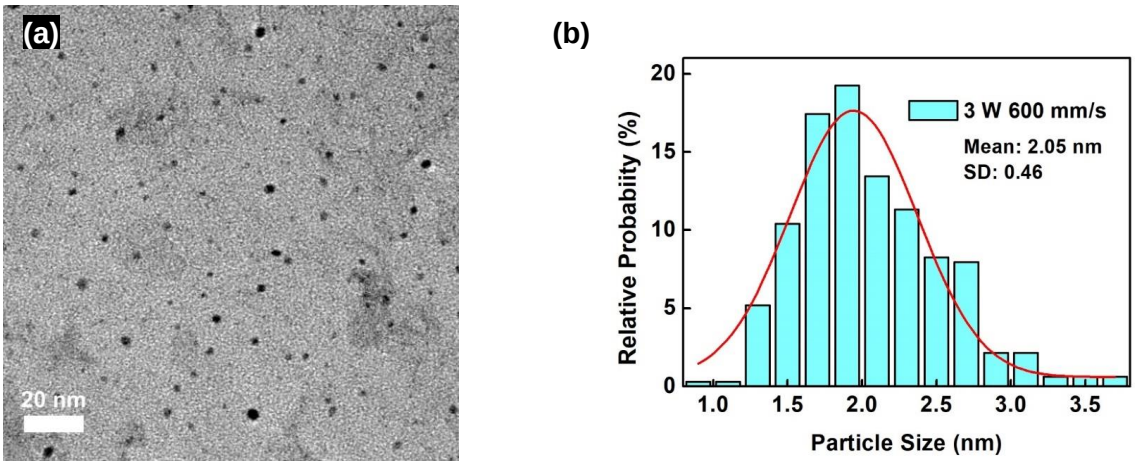

Figure S21. (a) TEM image and (b) particle size distribution analysis of Pt NPs supported on a few-layer graphene carbon network prepared using a LIFT process with a Pt source thickness of 5 nm, a laser power of 3 W, and a scribing speed of 600 mm/s.

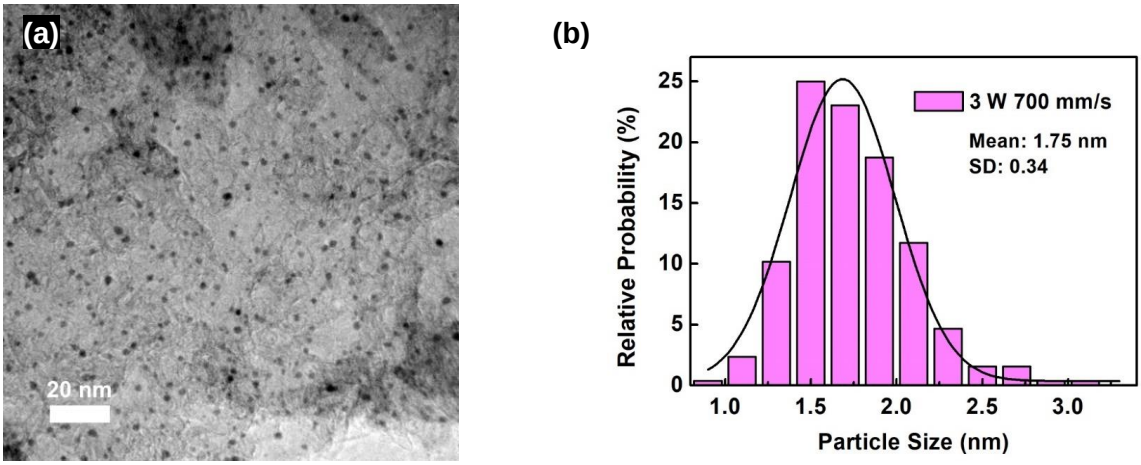

Figure S22. (a) TEM image and (b) particle size distribution analysis of Pt NPs supported on a few-layer graphene carbon network prepared using a LIFT process with a Pt source thickness of 5 nm, a laser power of 3 W, and a scribing speed of 700 mm/s.

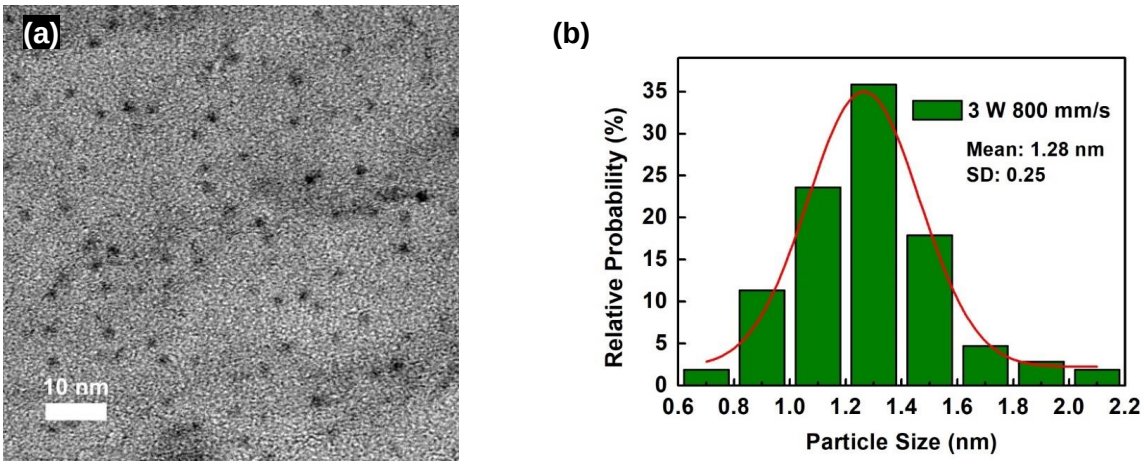

Figure S23. (a) TEM image and (b) particle size distribution analysis of Pt NPs supported on a few-layer graphene carbon network prepared using a LIFT process with a Pt source thickness of 5 nm, a laser power of 3 W, and a scribing speed of 800 mm/s.

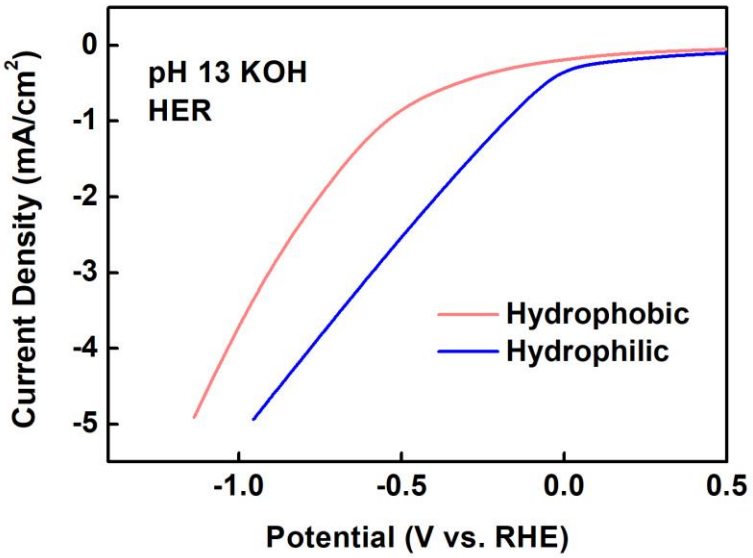

Figure S24. LSVs in N_2-saturated pH 13 KOH (100 mM) with a scan rate of 10 mV/s of Pt NPs supported on carbon prepared using LIFT with a laser power of 3 W, a scribing speed of 400 mm/s, and a source thickness of 5 nm with (blue) and without (salmon) a post-LIFT laser treatment.

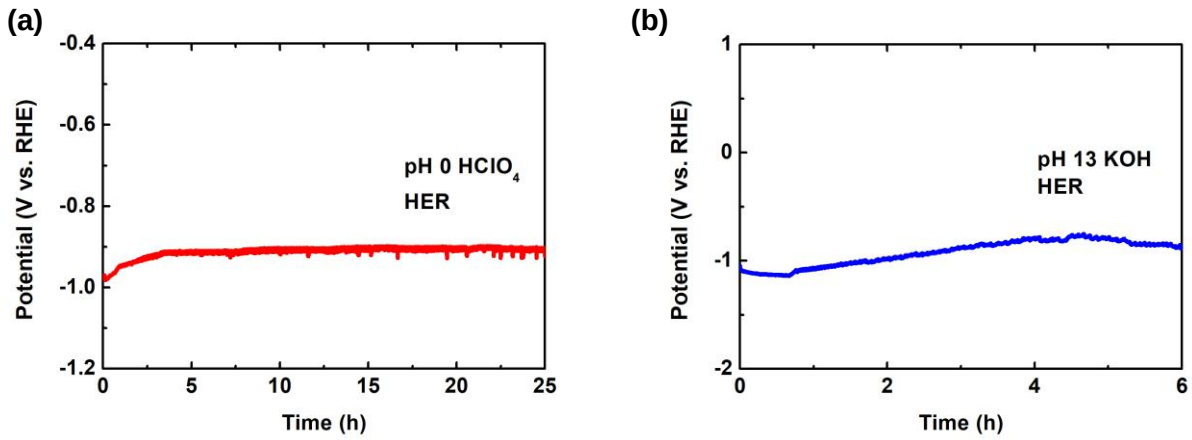

Figure S25. Long-term stability test through holding the current density passing through the working electrode at -5 mA/cm^2 of Pt NPs supported on carbon prepared using LIFT with a source thickness of 5 nm, a scribing speed of 400 mm/s, and a laser power of 3 W in N_2-saturated (a) pH 0 $HClO_4$ (1 M) and (b) pH 13 KOH (100 mM) solutions.

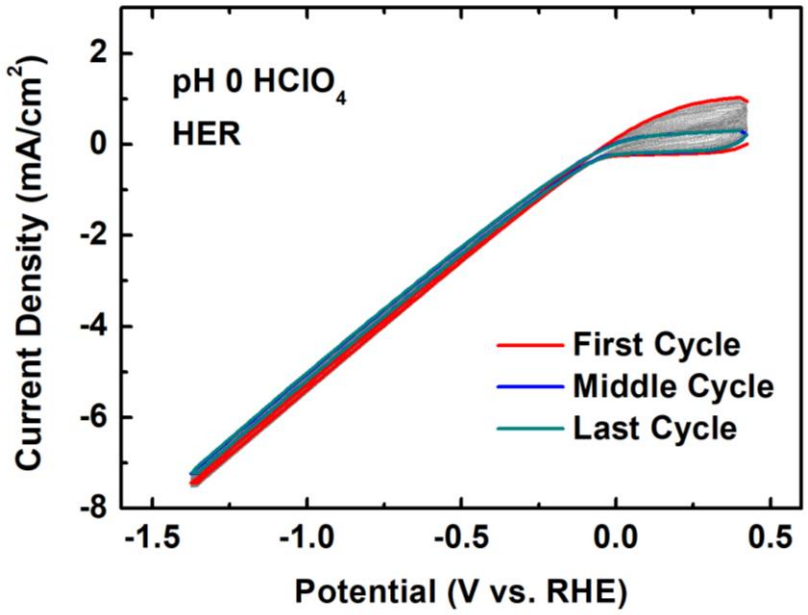

Figure S26. LSVs of Pt NPs supported on carbon prepared using LIFT with a source thickness of 5 nm, a scribing speed of 400 mm/s, and a laser power of 3 W in N_2-saturated pH 0 $HClO_4$ (1 M) with a scan rate of 100 mV/s for 2912 cycles, followed by 10 h soaking in N_2-saturated pH 0 $HClO_4$ (1 M) under open circuit potential with no current passing through the working electrode, then cycled for another 2912 cycles.

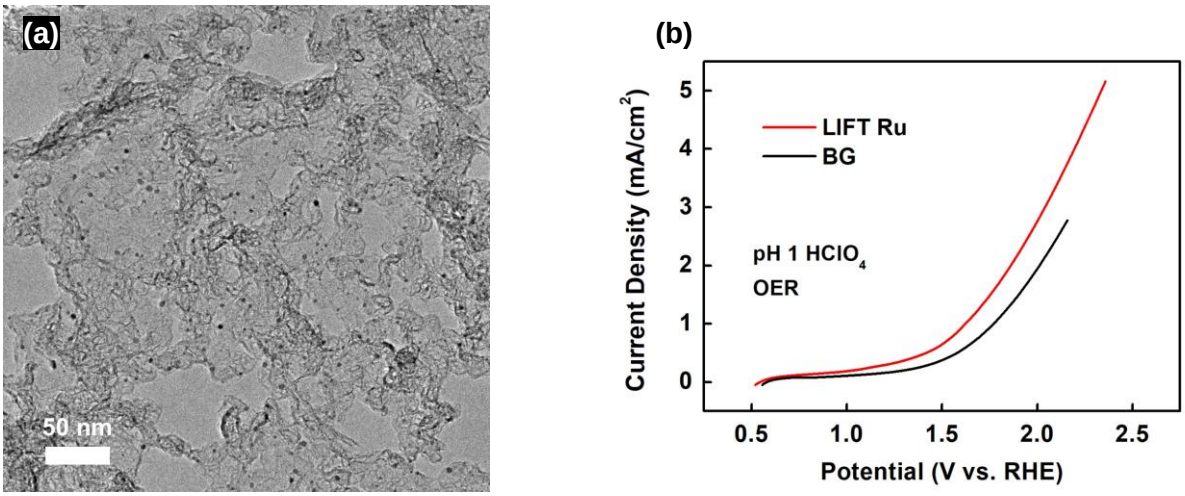

Figure S27. (a) TEM image and (b) LSVs recorded in N_2-saturated pH 1 $HClO_4$ (100 mM) with a scan rate of 10 mV/s (red line = LIFT Ru NPs, black line = LIFT carbon only) of Ru NPs (0.15 μg Ru/cm^2) supported on a few-layer graphene carbon network prepared using a LIFT process with a Ru source thickness of 5 nm, a laser power of 3 W, and a scribing speed of 400 mm/s.

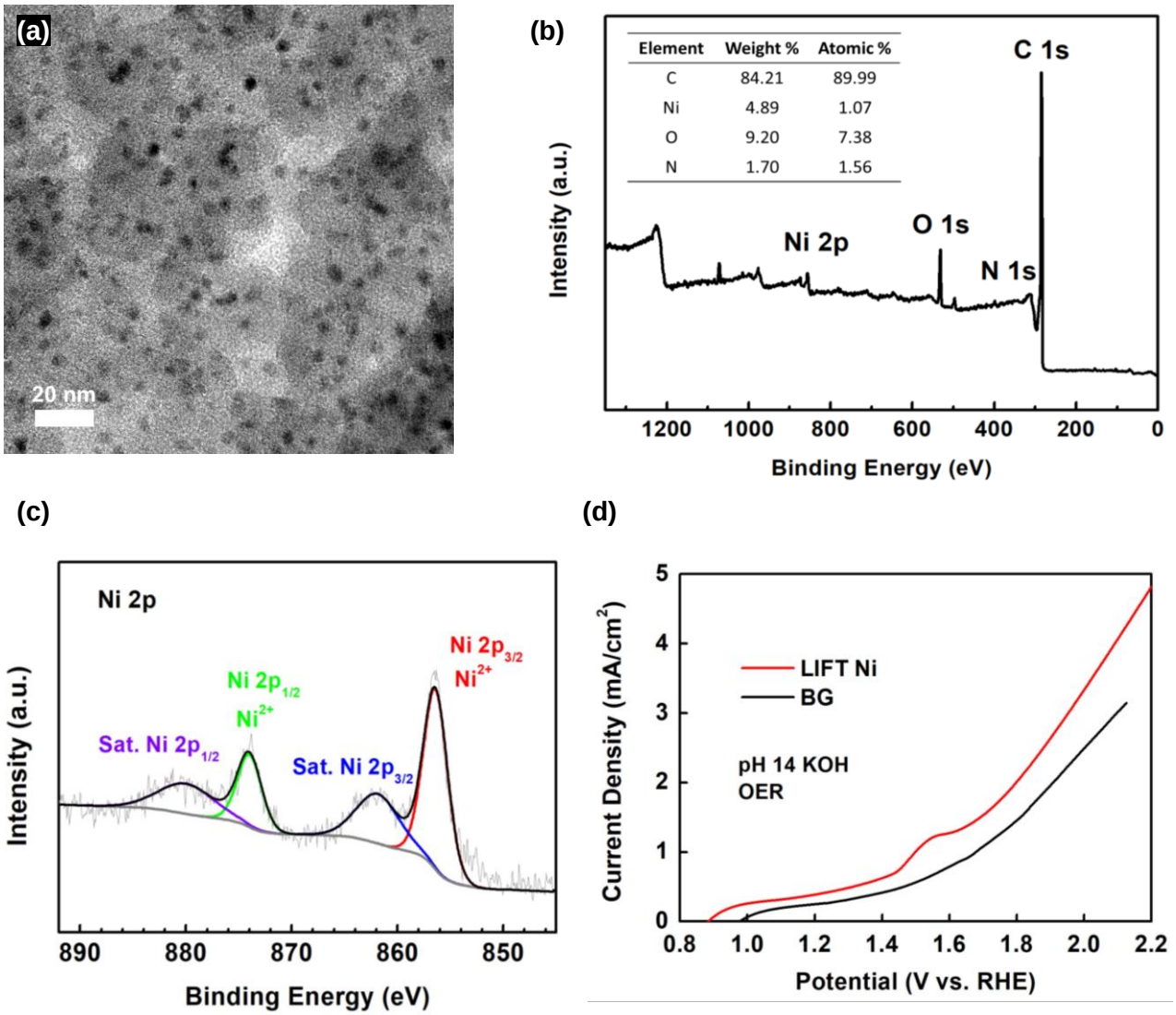

Figure S28. (a) TEM image, (b) XPS survey spectrum, (c) high-resolution XPS Ni 2p spectrum (gray = measured; red, blue, green, purple = individual fit components; and black = cumulative sum of individual fit components), and (d) LSVs recorded in N_2-saturated pH 14 KOH (1 M) with a scan rate of 10 mV/s (red line = LIFT Ni NPs, black line = LIFT carbon only) of Ni NPs (2.09 μg Ni/cm^2) supported on a few-layer graphene carbon network prepared using a LIFT process with a Ni source thickness of 5 nm, a laser power of 3 W, and a scribing speed of 400 mm/s.

Supplemental Tables

Laser Power (W)	Particle Size (nm)	Polydispersity Index (PDI)
2	5.28 ± 0.85	0.026
3	2.18 ± 0.43	0.039
4	2.04 ± 0.29	0.020

Table S1. Particle size distribution of Pt NPs supported on carbon prepared using LIFT with a Pt source thickness of 5 nm, a scribing speed of 400 mm/s, and a laser power varying between 2 W and 4 W.

Source Thickness (nm)	Particle Size (nm)	Polydispersity Index (PDI)
2	1.76 ± 0.37	0.045
5	2.18 ± 0.43	0.039
10	3.30 ± 0.68	0.043

Table S2. Particle size distribution of Pt NPs supported on carbon prepared using LIFT with a laser power of 3 W, a scribing speed of 400 mm/s, and a Pt source thickness varying between 2 nm and 10 nm.

Element	Weight %	Atomic %
C	84.68	90.01
O	10.53	8.04
N	1.28	1.17
Pt	3.51	0.23
Total	100	100

Table S3. Chemical composition quantified using XPS of Pt NPs supported on carbon prepared using LIFT with a Pt source thickness of 5 nm, a scribing speed of 400 mm/s, and a laser power of 2 W.

Element	Weight %	Atomic %
C	77.35	84.6
O	15.83	13.00
N	2.22	2.08
Pt	4.60	0.31
Total	100	100

Table S4. Chemical composition quantified using XPS of Pt NPs supported on carbon prepared using LIFT with a Pt source thickness of 5 nm, a scribing speed of 400 mm/s, and a laser power of 3 W.

Element	Weight %	Atomic %
C	80.36	87.70
O	12.32	10.09
N	1.97	1.84
Pt	5.36	0.36
Total	100	100

Table S5. Chemical composition quantified using XPS of Pt NPs supported on carbon prepared using LIFT with a Pt source thickness of 5 nm, a scribing speed of 400 mm/s, and a laser power of 4 W.

Element	Weight %	Atomic %
C	91.17	94.89
O	5.18	4.05
N	1.00	0.89
Pt	2.65	0.17
Total	100	100

Table S6. Chemical composition quantified using XPS of Pt NPs supported on carbon prepared using LIFT with a scribing speed of 400 mm/s, a laser power of 3 W, and a Pt source thickness of 2 nm.

Element	Weight %	Atomic %
C	80.56	88.79
O	10.44	8.64
N	2.22	2.10
Pt	6.78	0.46
Total	100	100

Table S7. Chemical composition quantified using XPS of Pt NPs supported on carbon prepared using LIFT with a scribing speed of 400 mm/s, a laser power of 3 W, a Pt source thickness of 10 nm.

Method	BG (S/m)	LIFT Pt (S/m)	Pt/Vulcan/PI (S/m)
AC (Bio-logic SP-150)	393 ± 1	467 ± 9	299 ± 3
DC (Multimeter)	137 ± 3	227 ± 9	109 ± 8

Table S8. AC and DC conductivity measurements of LIFT Pt NPs and commercially-available 10 wt% Pt on Vulcan XC-72 using electrochemical impedance spectroscopy (EIS) and a multimeter.

Scribing Speed (mm/s)	Particle Size (nm)	Polydispersity Index (PDI)
300	2.79 ± 0.36	0.017
400	2.18 ± 0.43	0.039
500	2.12 ± 0.46	0.047
600	2.05 ± 0.46	0.051
700	1.75 ± 0.34	0.037
800	1.28 ± 0.25	0.039

Table S9. Particle size distribution of Pt NPs supported on carbon prepared using LIFT with a laser power of 3 W, a Pt source thickness of 5 nm, and a scribing speed varying between 300 mm/s and 800 mm/s.

Scan Rate (mm/s)	Weight %
300	2.79
400	2.17
500	2.12
600	2.05
700	1.75
800	1.28

Table S10. Pt loading (wt%) quantified using XPS of Pt NPs supported on carbon prepared using LIFT with a Pt source thickness of 5 nm, a laser power of 3 W, and the scribing speed varying between 300 mm/s and 800 mm/s.